UNIVERSITÀ DEGLI STUDI DI TRIESTE

XXXI CICLO DEL DOTTORATO DI RICERCA IN

NANOTECNOLOGIE

MULTIDISCIPLINARY RESEARCH ON METHODS AND TECHNOLOGIES ENABLING THE MONITORING OF BACTERIAL BIOFILM GROWTH AND DISINFECTION

ING-IND/22 - SCIENZA E TECNOLOGIA DEI MATERIALI

CANDIDATE
LAURA SQUARCIA

PROGRAM COORDINATOR
PROF. LUCIA PASQUATO

THESIS SUPERVISOR
PROF. ORFEO SBAIZERO

CO-SUPERVISOR
CRISTINA BERTONI

ANNO ACCADEMICO 2017/2018

Contents

Abstract……1

Part I - Bacterial biofilms: Life in community……..3

Chapter 1 – Biofilms: bacteria on surfaces……5
Chapter 2 – Biosensing and monitoring……..15
Chapter 3 – References……...19

Part II – Mechanical study of biofilms of different ages……...25

Chapter 1 – Atomic force microscopy for mechanical studies……27
Chapter 2 – Materials and methods……35
Chapter 3 – Results and discussion……..39
Chapter 4 – Conclusions and perspectives……47
Chapter 5 – References……...49

Part III – Real-time monitoring of biofilm growth and disinfection……..51

Chapter 1 – The quarts crystal microbalance with dissipation module……53
Chapter 2 – Materials and methods……60
Chapter 3 – Results and discussion……..65
Chapter 4 – Conclusions and perspectives……77
Chapter 5 – References……...81

Part IV – Interaction between bacteria and silica nanoparticles……...83

Chapter 1 – Introduction……85
Chapter 2 – Materials and methods……89
Chapter 3 – Results and discussion……..93
Chapter 4 – Conclusions and perspectives……...101
Chapter 5 – References……103

Final considerations……..107

Acknowledgements……109

A mio padre,
per il suo ultimo
prezioso insegnamento.

Non si è fatti per essere invincibili,
Ma si può scegliere di essere coraggiosi.

Abstract

Biofilms are dangerous for human health in many situation, from hospital to daily life. As sustainability is one of the topics of highest interest and with an impact at global level, the optimization of disinfection treatments to reduce the environmental impact is needed. Sensing technologies can provide a mean to fulfil these requirements. Hence, sensing methods enabling the detection of biofilm in early stage of formation and able to perform a real-time monitoring are sought for more and more. Due to the need to address these topics to develop know-how on research capable to delivery results in the short to long term, this work was structured to carry out both cutting-edge and application-oriented research. Upon a state of the art analysis, the atomic force microscopy (AFM) has been identified as a promising technology to investigate bacterial biofilms. Mechanical analysis on biofilms at different stages has been performed on *P.fluorescens* biofilms from 7 days up to 43 days old, revealing that there is a relation between softness of the biofilm and its age. In addition, AFM topography investigation of early-stage *P.fluorescens* biofilms before and after exposure to silica nanoparticles of 4nm and 100 nm diameter has been performed, showing that an interaction occurs with visible modification in cell morphology. Coupled with AFM studies, a laboratory setup based on a quartz crystal microbalance (QCM) with dissipation module, capable of detecting in real-time both mass and viscoelastic changes of bacterial biofilms, has been created. Experiments conducted, by adopting and optimizing suitable protocols for bacterial growth, have shown that disinfection processes provided by different chemical compounds can be effectively monitored through frequency and dissipation measurements. If QCM-based systems are robust and compact, they can be affected by some issues due to operational conditions that would need to be taken into account in the design of a system based on this technology for practical application.

Part I

Bacterial biofilms: Life in community

Biofilms: bacteria on surface

1

After many years of research about microorganisms as planktonic cells, it is evident that in nature the life of microbes is mostly represented by community of cells associated with surfaces, known as biofilms. This kind of structure is complex and organized to respond easily to environmental conditions and to protect the bacterial cells included. In this chapter, the main properties of the biofilm structure will be illustrated, with particular attention to the different stages of its life-cycle.

1.1 Introduction to biofilms

After more than hundred years studying bacteria as planktonic cells, it is now clear that in nature their activity is chiefly associated to surfaces and this is the reason why many researches are currently focused on the biofilm form of bacterial growth. It has been proved that more than 99% of bacteria grow attached on various surfaces and create consortia between cells (single or mixed species) that are incorporated in an extracellular matrix. [1, 4] This ability of microorganisms permits to increase the resistance and the adaptability to many factors and external stresses that would impact badly on their activity (e.g. protozoan and bacterial predators, phage infections, antibacterial agents) [5-8].

Many studies were performed to understand bacterial biofilms and they were mainly focused on the use of genetic and microscopic techniques. In particular, it was possible to observe that the biofilm formation is a multi-step process that starts from the attachment of single cells to a surface and arrives to the formation of a mature and complex structure.

Many studies suggest that different parallel pathways are possible to lead to biofilm formation and dispersal among various species (or different strain of the same species), and it appears that the environmental conditions are determinant for the selection of the pathway. However, the endpoints (structural and functional) of the biofilms are similar and it is possible to describe a biofilm cycle of formation [1, 9, 10].

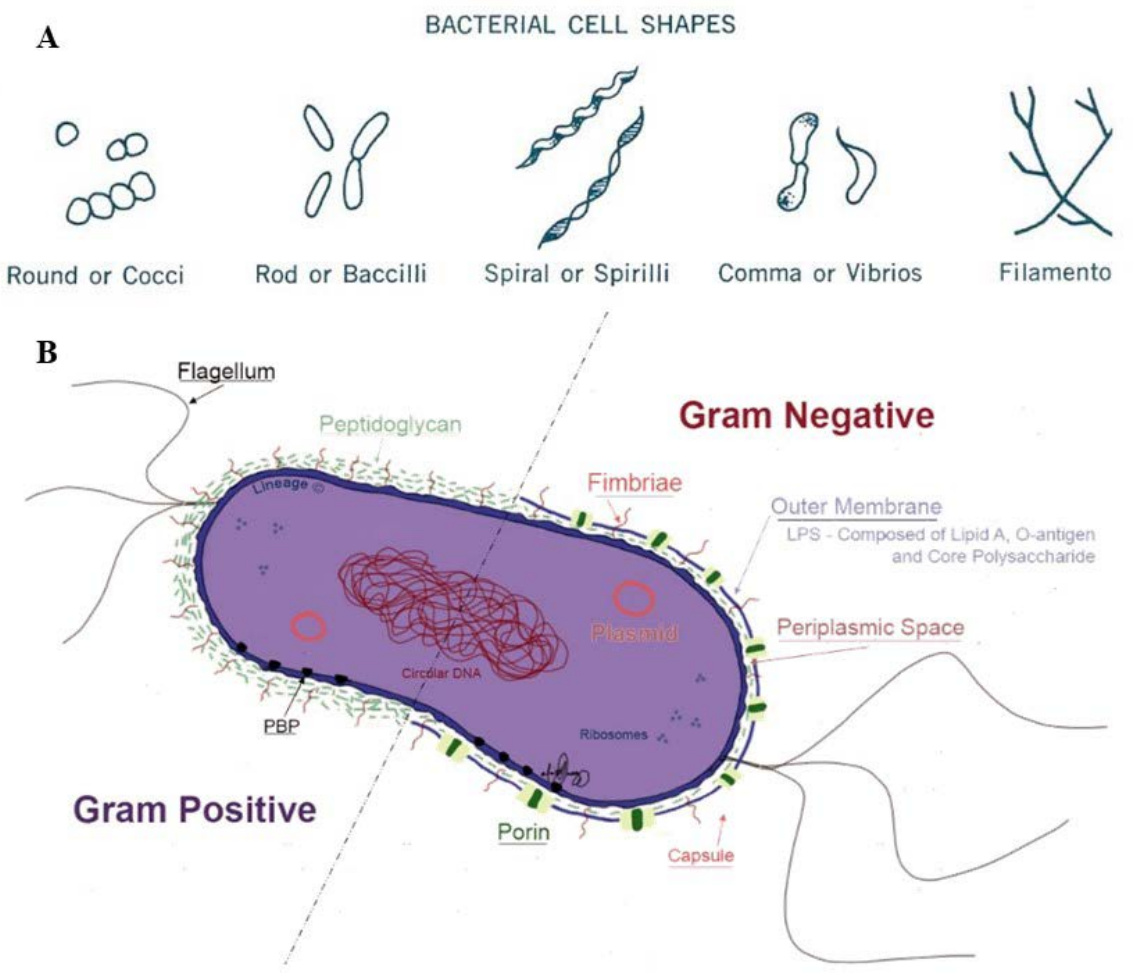

Figure 1.1 – (A) bacterial cell shapes [12] and (B) bacterial cell structure for Gram-positive and Gram-negative bacteria [13].

1.2 The bacterial structure

Bacteria are prokaryotic microorganisms that can have different shapes (such as bacillus and coccus; fig.1.1). An illustration of the bacterial cell structure is reported in fig. 1.2. The cytoplasmic membrane is a permeability barrier with

high selective functions. It consists of lipids and proteins that form a double layer: hydrophobic inside (between the two layers) and hydrophilic outside. This membrane has function of permeability, transport and energy production. Bacteria are also equipped with a cell wall formed by peptidoglycan. In addition to the cell wall, Gram-negative bacteria have an outer membrane (OM) composed by lipopolysaccharides, proteins and lipoproteins. Many prokaryotic cells have capsules, mucosal layers, flagella, pili, and fimbriae with different function as adhesion, gene transfer and motility. [11]

1.3 Biofilm formation and development

The first step of the formation of the biofilm is represented by cells that land to a surface (passively following gravity, Brownian motion or the flow of the liquid or actively using the swimming appendages) and start to attach. Then, they start to aggregate, grow and divide, producing a matrix that is composed mostly by polysaccharides. The biofilm continues to grow, it becomes mature, more resistant to external stresses and it starts to realise clumps of cells or individual cells that can start the cycle again.

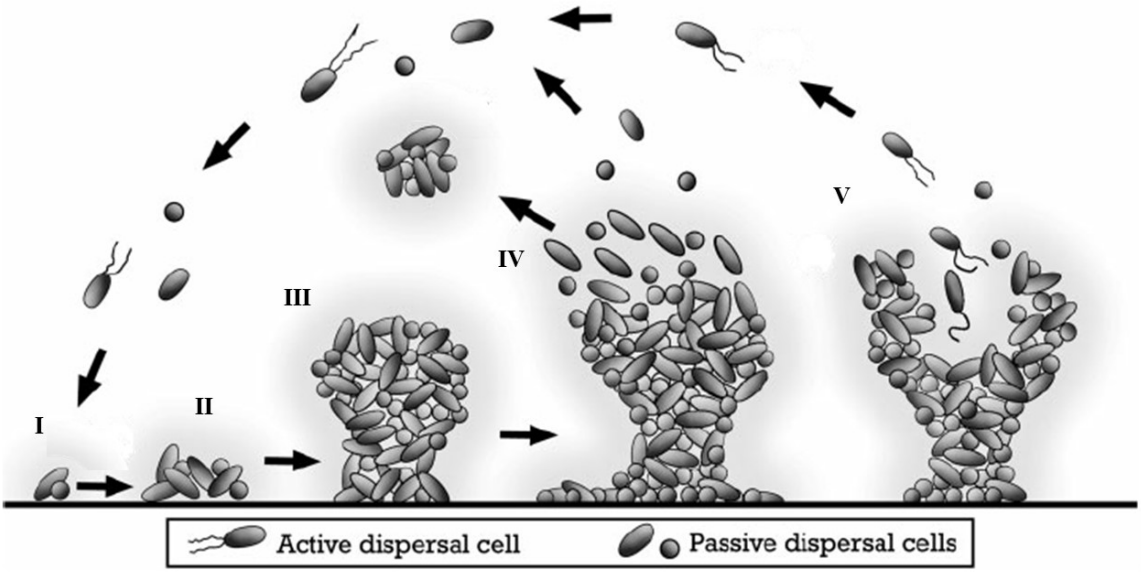

Figure 1.2 - Bacterial biofilm life-cycle [3]. Planktonic cells attach to a surface (I) and start to develop a biofilm (II). The mature biofilm releases passive (IV) and active (V) free cells or aggregates of cells that can start the cycle again.

1.4 The initial attachment to a surface

It has been observed that there are two stages in the attachment of bacteria to a surface. Pioneers of biofilms studies observed for different species that there was a first stage, in which the attachment of the cells to the surface was weak, and cells were able to rotate around the pole and also go back to planktonic phase, followed by a switch to an irreversible attachment along the longitudinal axes [12-14].
While the phenomenon of reversible and not-reversible attachment has been known since decades, a deep understanding of the molecular mechanisms that occur for these attachments lacks. However, adhesins and regulatory proteins were identified as part of the transition from the reversible to the irreversible phase of attachment [15-17].
Bacteria are capable to adhere to a great range of substrates. This adherence takes place throught bacterial appendages, extracellular polymers or by physicochemical interactions (electrostatic, Van der Walls, hydrophobic) [18].

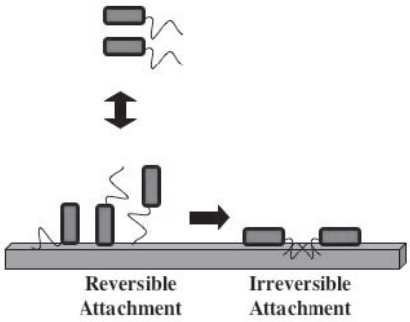

Figure 1.4 – Reversible and irreversible attachment of the cells to a surface [1]

1.5 The biofilm matrix

The extracellular matrix is an important component of a biofilm. It connects the cells giving also a protection against environmental factors, such as protozoan predation or immune response by the host in the case of medical domain [19-21].

Different materials are able to function as biofilm matrix, usually they are produced directly by the bacteria.

1.5.1 Extracellular polysaccharides

Extracellular polysaccharides are important components of biofilm matrix. The most common in biofilms of different bacterial species are cellulose, that appears to be associated with the capability to develop biofilms on abiotic surfaces (e.g. glass, polystyrene)[22, 23], PNAG/PIA, PSL and PEL, that have been found to be important respectively in the early stage and in the later stages of *P.aeruginosa* biofilm development [24, 25], and VPS.

1.5.2 Proteins

Proteins play a relevant role in the biofilm matrix. There are two important groups of proteins components in the matrix: multimeric cellular appendages and surface proteins.
Cellular appendages (flagella, fimbriae, pili) play an important role in biofilm formation both in the initial phases, promoting the transport and the adhesion of bacteria to a surface, and during the biofilm formation promoting cell-cell and cell-surface adhesion[26-35]. It has also been observed that many surface proteins (e.g. Ag43, AIDA, TibA, Bap, LapA) promote cell aggregation, surface adhesion and the subsequent biofilm formation[21, 36-38].

1.5.3 Extracellular DNA

Another group of components of the matrix is represented by extracellular DNA that may be able to interconnect compounds in different biofilms. The creation of long term relationship between the cells of a biofilm is important in order to exchange genetic material and form a stable film. [39-41].

The matrix is one of the most important parts of the biofilm because it represents the glue that bind all the components together, creating an interconnection between the cells that permits gene transfer. Depending on

the bacterial species and environmental conditions, different matrix-components are used to create it. There are evidences that the matrix is also a framework that permits the migration of bacteria within it [21].

1.6 Signaling in biofilms

The biofilm life-cycle is regulated by a set of signal transduction systems, both at intracellular and extracellular level. In particular, the detection of many environmental cues is essential to bring to modifications in bacterial cell physiology and gene expression[42].

At the intracellular level, it is determined that cyclic di-GMP (bis-(3'-5')-cyclic di-guanosine monophosphate) is a messenger in bacteria involved in regulation of processes that are related with biofilm formation and the behavior of the bacterial community. The mechanism of action of cyclic di-GMP is still almost unknown. In 1987 its allosteric activation in cellulose activity was described by Ross et al. [43], while its role as a signaling molecule has been appreciated relatively recently. [42, 44]

In order to coordinate the bacterial behavior within a community, the most useful strategy is the quorum sensing. The quorum sensing not only influences the development of a biofilm, its integrity and its architecture, but also arranges the timing and release of toxins against predators and host protection mechanisms [45-48]. For example, the role of different signals, such as N-acyl homoserine, indoles, hydroxylated indoles, and epinephrine, has been studied in *E. coli*, showing that these signals provide to the microorganism the capacity to monitor the presence of other cells (its own specie or other) and the activity of the host [49].

There are evidences of interaction between peptide signaling, bacterial products and cell density, these interactions are part of the system that regulates the biofilm cycle during its phases. In planktonic cell cultures, the expression of cell surface adhesins takes place during early growth when both density of cells and peptide signal concentrations are low. In the case of biofilms, the behaviour is similar when early stage-cell density is low and the nutrients are not limiting. When the density of cells increases, and the nutrient supply is narrow, the concentration of signals is high and may conduce to cell detachment and dispersion. The disseminated cells detect low

signal concentration and promote the expression of adhesins to be able to colonize new sites (fig. 1.4) [2].

1.7 Dispersal in biofilms

There are passive processes that promote the dispersion of cells from biofilms, due for example to the erosion by fluid shear, however biofilms can perform an active release of free-swimming planktonic cells. The investigation of the mechanism that leads to the dispersal in biofilm are at the beginning, but there are some that are already known such as the enzyme-mediated breakdown of the matrix, surfactant production, intracellular signaling, quorum sensing, and the presence of nitric oxide, as recently observed in the case of *P. aeruginosa*. It appears that the release of active cells takes place from the center of mature biofilm structures, leaving cavities behind. This process is often associated with the lysis of biofilm's subcommunities of cells [50].

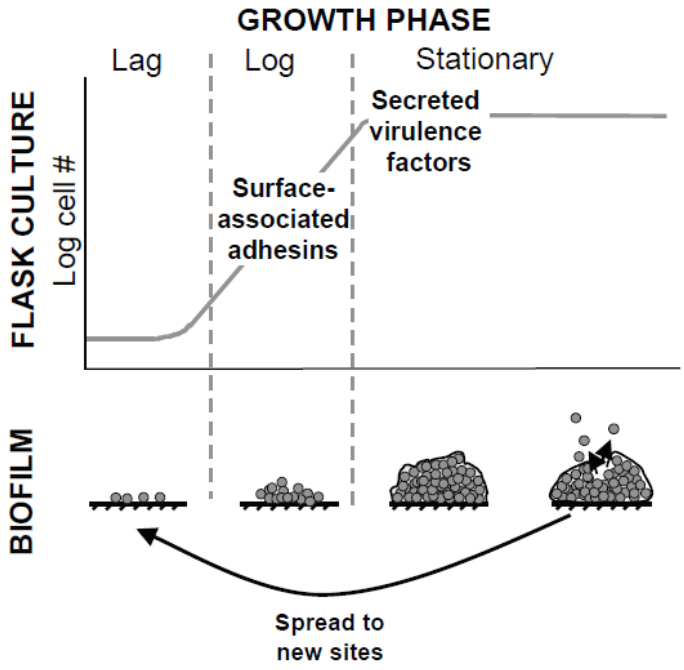

Figure 1.4 – expression of cell surface adhesins and cell dispersion in the different phases of growth. Similarity between biofilms and flask culture [2]

1.8 Resistance against predation and disinfection

The biofilm form of bacteria appears to provide a better resistance against phagocytic predators to the cells. In the case of biofilms associated with hosts, the resistance is developed against both host defenses and antimicrobial compounds.
Bacterial predators in various ecosystems are the protozoa (phagotrophic microeukaryotes), while the human hosts have innate defenses, however in both cases the process is phagocytosis. Even if the knowledge concerning the predator-prey interaction still has many gaps, it appears, in general, that the biofilm life-style gives more possibilities of survival than the planktonic form. [51, 52]

1.8.1 Protection mechanisms

Biofilms have specific features that appears to be responsible of the resistance to phagocytic assaults.
It appears that adherent bacteria are more exposed to predators as the sessile communities have no escape options, this issue leads to the development of protective features during biofilm composition [51, 53].
An important role is played by the matrix that represent a physical barrier and helps the formation of clusters of cells that are harder to be attacked by the predators, compare to single cells. It also works as a diffusional barrier that interfere with antibacterial compounds. [51, 54, 55] For example, experiments that were performed in order to investigate the penetration of chlorine into biofilms allowed to observe that the compound penetration was limited to the first layers of the biofilm [56, 57].
The limited penetration of biocides is probably due to the fact that, as they are highly chemically reactive, they interact easily with the matrix constituents.
The biofilm condition can also favor the development of different phenotypes that apparently helps the biofilm to become more resistant to environmental stresses. It has to be taken into account that as the penetration of a biocide is limited, the cells that are in the inner layer will be exposed just to a low quantity of antimicrobial compound that will be not lethal, resulting in an adaptive process of the cells to that specific agent [58-60].

The community embedded in the matrix is represented by a high concentration of cells that are able to communicate and collaborate (quorum sensing) [61], this condition permits a fast response to the modification of the environment conditions, also because of gene transfer that confer specific features, antimicrobial resistance included.

1.9 Concluding remarks

Bacterial cells can grow both in planktonic and biofilm form. In nature, more than 99% of bacteria grow adherent to various substrates and create consortia between cells that are embedded in an extracellular matrix. The biofilm is a complex structure within the cells are able to communicate and collaborate allowing the structure to be more resistant against predation and external stresses, and to adapt easily to environmental modifications.

Biosensing and monitoring

2

Bacterial biofilms represent an important problem in many situations, from hospitals [62] to daily life [63]. The formation of biofilms has in fact implications at medical, environmental and industrial level. The biofilm mode of life gives to microorganism higher resistance to antibiotics, biocides and UV light. According to national and international organizations (WHO, EFSA, ISS), 80% of disease caused by bacteria, including those caused by food and contaminated water, are due to biofilms. Detection and disinfection systems for household use are more and more sought because of to poor quality of potable water around the world [64-67]. In different fields, when there are hygiene and sanitary risks, the interventions consist in the application of extraordinary disinfection procedures that may have bad consequences for the environment or involve damage to implants. For all these reasons, research at both academic and industrial levels, is looking for systems capable of detecting microorganisms around us to make disinfection more effective and efficient [68, 69].

An overview of the state of the art shows that different techniques are available to detect bacteria both in planktonic and biofilm form. Many of those techniques present limitations, like for example being able to detect a specific property of a certain strain, or in the case of biofilms, being sensible to a biofilm once this is already mature [70]. Other methods, such as bioluminescence or fluorimetry, are usually applicable just in the laboratory, because they may require sample manipulation (e.g. genetic modification of microorganisms, dye labelling).

In table 2.1 sensing techniques, grouped by the physical or chemical principle on which they are based, are reported, with the related detection limits available in literature. Depending on the technique, the detection limit is reported as thickness or density of cells per unit area.

In laboratory research, detecting and monitoring technologies based on a specific property of a microorganism are wildly used. However, in order to be applicable to all the contamination that may occur in different fields, a detecting system has to be sensible to properties that are common to a range of microorganisms (not-specific properties).

A real-time monitoring leads to an improvement of disinfection systems, optimizing the quantity of the bactericidal compound and the duration of the treatment, with the lowest environmental impact.

Some commercial devices are available, for example ALVIM™ System (Genoa) [71] and BIoGEORGE™ (USA) [72]. These devices are based on electrochemical methods and are designed to be applied in big industrial systems. Both cost and application requirements make these systems not suitable for point-of-use water treatment systems, or household appliances, that are also susceptible to biofilm formation with potential dangerous consequences for human health [63].

Furthermore, it must be reminded that bacteria are able to develop a resistance to chemical compounds, and this phenomenon requires long-term monitoring to assess actual disinfection treatment performances over the time. In this regard, an example of cutting-edge research concerning the long-term monitoring of a biofilm is reported by Shen et al. [73]. In this study, the response of a biofilm in terms of stiffness to a long-term chlorine exposure is monitored using the atomic force microscopy. During the first month of disinfection, the biofilm becomes more rigid and this behavior corresponds to a decrease in thickness. Subsequently, along the second and third months of exposure to chlorine the biofilm exhibits a resistance development, with an increase in thickness and a decrease in stiffness back to initial levels. This is an example of how the mechanical properties can be monitored to get information about the “health” of a biofilm.

Table 2.1 Main methods for biosensing (modified from the table of Melo et al. [70])

	Method	Info on biofilm	Detection limit	Notes
Detection of radiation signals	Bioluminescence	Biological activity, composition	-	Organisms that naturally emit light or genetically manipulated. Applicability under non-lab conditions limited
	Fluorometry	Biological activity, composition	-	Enviromental factors influence the readings; photodegradation; quenching; cascade effect
	Spectroscopy IR	Composition	-	-
	Attenuated total internal reflection – Evanescent Waves	Surface coverage	$5x10^5$ cells cm^2	Limited to a thin layer~1µm
	Attenuated total internal reflection – Surface Plasmon Resonance	Surface coverage	-	Limited to a thin layer
	Nuclear magnetic resonance spectroscopy (NMR)	Physical structure; composition	-	Unhandy and expensive equipment; the use of NMR outside laboratories is not common
	Photoacoustic spectroscopy	Physical structure; composition Thickness and homogenity of a biofilm	10 µm depth resolution	Questionable whether the speed of sound is identical in bulk liquid and biofilm
Deposit measurements	Differential turbidity	Thickness	100 µm	Mature biofilm
	Fiber optical device	Surface coverage	10^5 cells cm^2	Not appropiate for thick biofilms
	Heat transfer	Heat resistance	-	Not enough sensitivity to detect the initial attachment
	Pressure drop	Thickness	-	Mature biofilm
	Metabolic products	Biological activity, composition	-	-
Electric signals	Electrochemical techniques (MIC-electrodes)	Biological activity Chemical conditions within biofilms (pH, oxygen concentration…)	-	Use in industrial conditions (significant signal drift requires frequent calibration)
	Impedance measurements	Thickness	200 µm	Results not easy to interpret; application limited to laboratory
	Capacitance measurements	Surface coverage	10^8 cells cm^2	-
Vibration signals	QCM	Surface coverage	3×10^5 cells cm^2	-
	Ultrasonic reflectometry	Exopolysaccharides (EPS) concentration in liquid phase	-	Mature biofilm

This PhD work extended the use of atomic force microscopy to assess the toxic effect of silica nanoparticles to early stage-biofilms, and to investigate the relation between age and mechanical properties of *P.fluorescens* biofilms. Furthermore, a sensing technique, based on a quartz crystal microbalance equipped with a module to measure the dissipation, was used for a real-time monitoring to gain information about the growth of biofilms and their response to disinfection treatments.

Besides, most of the literature on the use of QCM to monitor biofilm growth and disinfection considers the use of standard chemicals. For this reason, in order to compare results of this part of the work with the state-of-the art, the experiments were carried out using standard disinfectants for potable water applications and for medical sterilization.

References 3

1. Givskov, S.K.a.M., *The Biofilm Mode of Life: Mechanisms and Adaptations*. 2007: Horizon Bioscience.
2. Yarwood, J.M., *Peptide Signaling*. The Biofilm Mode of Life: Mechanisms and Adaptations, eds Kjelleberg S, Givskov M, (Horizon Bioscience, Norfolk, UK), 2007: p. pp 141-164.
3. Steinberg, P.D., et al., *Interfaces Between Bacterial and Eukaryotic "Neuroecology"*. Integrative and Comparative Biology, 2011. **51**(5): p. 794-806.
4. Donlan, R.M. and J.W. Costerton, *Biofilms: Survival Mechanisms of Clinically Relevant Microorganisms*. Clinical Microbiology Reviews, 2002. **15**(2): p. 167-193.
5. Matz, C., et al., *Microcolonies, quorum sensing and cytotoxicity determine the survival of Pseudomonas aeruginosa biofilms exposed to protozoan grazing*. Environmental Microbiology, 2004. **6**(3): p. 218-226.
6. Patel, R., *Biofilms and Antimicrobial Resistance*. Clinical Orthopaedics and Related Research®, 2005. **437**: p. 41-47.
7. Picioreanu, C., M.C.M. Van Loosdrecht, and J.J. Heijnen, *Effect of diffusive and convective substrate transport on biofilm structure formation: A two-dimensional modeling study*. Biotechnology and Bioengineering, 2000. **69**(5): p. 504-515.
8. Sutherland, I.W., et al., *The interaction of phage and biofilms*. FEMS Microbiology Letters, 2004. **232**(1): p. 1-6.
9. Auschill, T.M., et al., *Spatial distribution of vital and dead microorganisms in dental biofilms*. Archives of Oral Biology, 2001. **46**(5): p. 471-476.
10. Hope, C.K., D. Clements, and M. Wilson, *Determining the spatial distribution of viable and nonviable bacteria in hydrated microcosm dental plaques by viability profiling*. Journal of Applied Microbiology, 2002. **93**(3): p. 448-455.

11. Madigan, M.T., T.D. Brock, and F. Baldi, *Brock. Biologia dei microrganismi. Ediz. illustrata*. 2012: Pearson.
12. MARSHALL, K.C., R. STOUT, and R. MITCHELL, *Mechanism of the Initial Events in the Sorption of Marine Bacteria to Surfaces*. Microbiology, 1971. **68**(3): p. 337-348.
13. Lawrence, J.R., et al., *Behavior ofPseudomonas fluorescens within the hydrodynamic boundary layers of surface microenvironments*. Microbial Ecology, 1987. **14**(1): p. 1-14.
14. Zobell, C.E., *The Effect of Solid Surfaces upon Bacterial Activity*. Journal of Bacteriology, 1943. **46**(1): p. 39-56.
15. Caiazza, N.C. and G.A. O'Toole, *SadB Is Required for the Transition from Reversible to Irreversible Attachment during Biofilm Formation by Pseudomonas aeruginosa PA14*. Journal of Bacteriology, 2004. **186**(14): p. 4476-4485.
16. Hinsa, S.M., et al., *Transition from reversible to irreversible attachment during biofilm formation by Pseudomonas fluorescens WCS365 requires an ABC transporter and a large secreted protein*. Molecular Microbiology, 2003. **49**(4): p. 905-918.
17. Espinosa-Urgel, M., A. Salido, and J.-L. Ramos, *Genetic Analysis of Functions Involved in Adhesion of Pseudomonas putida to Seeds*. Journal of Bacteriology, 2000. **182**(9): p. 2363-2369.
18. Daniel P. MacEachran, G.A.O.T., *Do not fear commitment: the initial transition to a surface lifestyle by Pseudomonas*. The Biofilm Mode of Life: Mechanisms and Adaptations, eds Kjelleberg S, Givskov M, (Horizon Bioscience, Norfolk, UK), 2007: p. pp 23-35.
19. Matz, C. and S. Kjelleberg, *Off the hook – how bacteria survive protozoan grazing*. Trends in Microbiology, 2005. **13**(7): p. 302-307.
20. Costerton, J.W., P.S. Stewart, and E.P. Greenberg, *Bacterial Biofilms: A Common Cause of Persistent Infections*. Science, 1999. **284**(5418): p. 1318.
21. Pamp SJ, G.M., Tolker-Nielsen T, *The biofilm matrix: A sticky framework*. The Biofilm Mode of Life: Mechanisms and Adaptations, eds Kjelleberg S,Givskov M, (Horizon Bioscience, Norfolk, UK) 2007: p. pp 37–69.
22. García, B., et al., *Role of the GGDEF protein family in Salmonella cellulose biosynthesis and biofilm formation*. Molecular Microbiology, 2004. **54**(1): p. 264-277.
23. Zogaj, X., et al., *The multicellular morphotypes of Salmonella typhimurium and Escherichia coli produce cellulose as the second component of the extracellular matrix*. Molecular Microbiology, 2001. **39**(6): p. 1452-1463.
24. Friedman, L. and R. Kolter, *Two Genetic Loci Produce Distinct Carbohydrate-Rich Structural Components of the Pseudomonas aeruginosa Biofilm Matrix*. Journal of Bacteriology, 2004. **186**(14): p. 4457-4465.

25. Vasseur, P., et al., *The pel genes of the Pseudomonas aeruginosa PAK strain are involved at early and late stages of biofilm formation.* Microbiology, 2005. **151**(3): p. 985-997.
26. O'Toole, G.A. and R. Kolter, *Flagellar and twitching motility are necessary for Pseudomonas aeruginosa biofilm development.* Molecular Microbiology, 1998. **30**(2): p. 295-304.
27. O'Toole, G.A. and R. Kolter, *Initiation of biofilm formation in Pseudomonas fluorescens WCS365 proceeds via multiple, convergent signalling pathways: a genetic analysis.* Molecular Microbiology, 1998. **28**(3): p. 449-461.
28. Klausen, M., et al., *Biofilm formation by Pseudomonas aeruginosa wild type, flagella and type IV pili mutants.* Molecular Microbiology, 2003. **48**(6): p. 1511-1524.
29. Watnick, P.I. and R. Kolter, *Steps in the development of a Vibrio cholerae El Tor biofilm.* Molecular microbiology, 1999. **34**(3): p. 586-595.
30. Yamada, M., A. Ikegami, and H.K. Kuramitsu, *Synergistic biofilm formation by Treponema denticola and Porphyromonas gingivalis.* FEMS Microbiology Letters, 2005. **250**(2): p. 271-277.
31. Gilbert, P., D.J. Evans, and M.R.W. Brown, *Formation and dispersal of bacterial biofilms in vivo and in situ.* Journal of Applied Bacteriology, 1993. **74**(S22): p. 67S-78S.
32. Duguid, J.P., E.S. Anderson, and I. Campbell, *Fimbriae and adhesive properties in Salmonellae.* J Pathol Bacteriol, 1966. **92**(1): p. 107-38.
33. Pratt, L.A. and R. Kolter, *Genetic analysis of Escherichia coli biofilm formation: roles of flagella, motility, chemotaxis and type I pili.* Mol Microbiol, 1998. **30**(2): p. 285-93.
34. Schembri, M.A. and P. Klemm, *Biofilm Formation in a Hydrodynamic Environment by Novel FimH Variants and Ramifications for Virulence.* Infection and Immunity, 2001. **69**(3): p. 1322-1328.
35. Ghigo, J.M., *Natural conjugative plasmids induce bacterial biofilm development.* Nature, 2001. **412**(6845): p. 442-5.
36. Henderson, I.R., M. Meehan, and P. Owen, *Antigen 43, a phase-variable bipartite outer membrane protein, determines colony morphology and autoaggregation in Escherichia coli K-12.* FEMS Microbiol Lett, 1997. **149**(1): p. 115-20.
37. Danese, P.N., et al., *The outer membrane protein, antigen 43, mediates cell-to-cell interactions within Escherichia coli biofilms.* Mol Microbiol, 2000. **37**(2): p. 424-32.
38. Lasa, I. and J.R. Penades, *Bap: a family of surface proteins involved in biofilm formation.* Res Microbiol, 2006. **157**(2): p. 99-107.
39. Li, Y.H., et al., *Natural genetic transformation of Streptococcus mutans growing in biofilms.* J Bacteriol, 2001. **183**(3): p. 897-908.
40. Wang, B.Y., B. Chi, and H.K. Kuramitsu, *Genetic exchange between Treponema denticola and Streptococcus gordonii in biofilms.* Oral Microbiol Immunol, 2002. **17**(2): p. 108-12.

41. Hendrickx, L., M. Hausner, and S. Wuertz, *Natural genetic transformation in monoculture Acinetobacter sp. strain BD413 biofilms.* Appl Environ Microbiol, 2003. **69**(3): p. 1721-7.
42. John M. Dow, Y.F., Jean. Lucey, and Robert P. Ryan, *Cyclic di-GMP as an Intracellular Signal Regulating Bacterial biofilm Formation*

The Biofilm Mode of Life: Mechanisms and Adaptations, eds Kjelleberg S,Givskov M, (Horizon Bioscience, Norfolk, UK) 2007: p. pp 71-93.
43. Ross, P., et al., *Regulation of cellulose synthesis in Acetobacter xylinum by cyclic diguanylic acid.* Nature, 1987. **325**: p. 279.
44. D'Argenio, D.A. and S.I. Miller, *Cyclic di-GMP as a bacterial second messenger.* Microbiology, 2004. **150**(Pt 8): p. 2497-502.
45. Salmond, G.P., et al., *The bacterial 'enigma': cracking the code of cell-cell communication.* Mol Microbiol, 1995. **16**(4): p. 615-24.
46. Williams, P., et al., *Quorum sensing and the population-dependent control of virulence.* Philosophical transactions of the Royal Society of London. Series B, Biological sciences, 2000. **355**(1397): p. 667-680.
47. Swift, S., et al., *Quorum sensing as a population-density-dependent determinant of bacterial physiology.* Adv Microb Physiol, 2001. **45**: p. 199-270.
48. Steve Atkinson, M.C., and Paul Williams, *N-Acylhomoserine Lactones, Quorum Sensing, and Biofilm Development in Gram-negative Bacteria.* The Biofilm Mode of Life: Mechanisms and Adaptations, eds Kjelleberg S, Givskov M, (Horizon Bioscience, Norfolk, UK), 2007: p. pp 95-122.
49. Bentley, T.K.W.a.W.E., *Signaling in Escherichia coli biofilms.* The Biofilm Mode of Life: Mechanisms and Adaptations, eds Kjelleberg S, Givskov M, (Horizon Bioscience, Norfolk, UK), 2007: p. pp 123-139.
50. Webb, J.S., *Differentiation and dispersal in biofilms.* The Biofilm Mode of Life: Mechanisms and Adaptations, eds Kjelleberg S, Givskov M, (Horizon Bioscience, Norfolk, UK), 2007: p. pp 165-174.
51. Matz, C., *Biofilms as Refuge against Predation.* The Biofilm Mode of Life: Mechanisms and Adaptations, eds Kjelleberg S, Givskov M, (Horizon Bioscience, Norfolk, UK), 2007: p. pp 195-213.
52. Matz, C., et al., *Biofilm formation and phenotypic variation enhance predation-driven persistence of Vibrio cholerae.* Proc Natl Acad Sci U S A, 2005. **102**(46): p. 16819-24.
53. Duffy, J.E. and M.E. Hay, *Seaweed Adaptations to Herbivory.* BioScience, 1990. **40**(5): p. 368-375.
54. Bylund, J., et al., *Exopolysaccharides from Burkholderia cenocepacia inhibit neutrophil chemotaxis and scavenge reactive oxygen species.* J Biol Chem, 2006. **281**(5): p. 2526-32.
55. Vuong, C., et al., *Polysaccharide intercellular adhesin (PIA) protects Staphylococcus epidermidis against major components of the human innate immune system.* Cell Microbiol, 2004. **6**(3): p. 269-75.
56. De Beer, D., R. Srinivasan, and P.S. Stewart, *Direct measurement of chlorine penetration into biofilms during disinfection.* Appl Environ Microbiol, 1994. **60**(12): p. 4339-44.

57. Jang, A., et al., *Measurement of chlorine dioxide penetration in dairy process pipe biofilms during disinfection.* Appl Microbiol Biotechnol, 2006. **72**(2): p. 368-76.
58. Sauer, K., et al., *Pseudomonas aeruginosa displays multiple phenotypes during development as a biofilm.* J Bacteriol, 2002. **184**(4): p. 1140-54.
59. McCann, K.S., *The diversity–stability debate.* Nature, 2000. **405**: p. 228.
60. Bridier, A., et al., *Resistance of bacterial biofilms to disinfectants: a review.* Biofouling, 2011. **27**(9): p. 1017-32.
61. Parsek, M.R. and E.P. Greenberg, *Sociomicrobiology: the connections between quorum sensing and biofilms.* Trends Microbiol, 2005. **13**(1): p. 27-33.
62. Parsek, M.R. and P.K. Singh, *Bacterial biofilms: An emerging link to disease pathogenesis.* Annual Review of Microbiology, 2003. **57**: p. 677-701.
63. Zalar, P., et al., *Dishwashers - A man-made ecological niche accommodating human opportunistic fungal pathogens.* Fungal Biology, 2011. **115**(10): p. 997-1007.
64. Berry, D., C.W. Xi, and L. Raskin, *Microbial ecology of drinking water distribution systems.* Current Opinion in Biotechnology, 2006. **17**(3): p. 297-302.
65. Ponce-Terashima, R., et al., *Sources and Distribution of Surface Water Fecal Contamination and Prevalence of Schistosomiasis in a Brazilian Village.* Plos Neglected Tropical Diseases, 2014. **8**(10).
66. Wang, J.F., et al., *Spatiotemporal Transmission and Determinants of Typhoid and Paratyphoid Fever in Hongta District, Yunnan Province, China.* Plos Neglected Tropical Diseases, 2013. **7**(3): p. 9.
67. Mulamattathil, S.G., C. Bezuidenhout, and M. Mbewe, *Analysis of physico-chemical and bacteriological quality of drinking water in Mafikeng, South Africa.* Journal of water and health, 2015. **13**(4): p. 1143-52.
68. Miles, S.L., et al., *Evaluation of Select Sensors for Real-Time Monitoring of Escherichia coli in Water Distribution Systems.* Applied and Environmental Microbiology, 2011. **77**(8): p. 2813.
69. http://www.itramhigiene.com/en/.
70. Melo, P.J.L.F., *Online biofilm monitoring.* Environmental Science and Bio/Technology, 2003: p. 269-283.
71. http://www.alvimcleantech.com/cms/it/.
72. http://www.alspi.com/biogeorge.htm.
73. Shen, Y., et al., *Response of Simulated Drinking Water Biofilm Mechanical and Structural Properties to Long-Term Disinfectant Exposure.* Environmental Science & Technology, 2016. **50**(4): p. 1779-1787.

Part II

Mechanical study of biofilms of different ages

1 Atomic force microscopy for mechanical studies

The atomic force microscopy is a scanning probe technology that enables the study of solids with nanometric resolution. The interactions between probe and sample permit the acquisition of information about sample morphology and its mechanical properties. In this chapter, a description of principles and functioning of this technique and its application for the mechanical study of bacterial biofilms are illustrated.

1.1 Principles and technology

An atomic force microscope (AFM) uses a probe, constituted by a cantilever and a tip, whose characteristics can be chosen depending on the sample to analyse and the measurements to perform. The forces involved in the interaction between tip and sample (in the order of $10^{-13} – 10^{-6}$ N) can be van der Waals, ionic repulsion, friction forces, adhesion forces, electrostatic forces and magnetostatics forces. Due to these forces, the cantilever deflects, and this deflection is used to get information about the sample.
The deformation of the cantilever has a linear elastic behaviour, following Hooke's law, and its measurements are very precise [3, 4].

$$F = -k \Delta z \quad (1.1)$$

The equation 1.1 describes Hooke's low: F is the applied force, k is the elastic constant and Δz is the vertical deflection of the cantilever due to the interaction with the sample.
Usually, a laser light is reflected off the rear of the cantilever and then collected by a photodiode detector that produces an output signal (proportional to the cantilever deflection). A differential amplifier collects the detector's output signal and the information is then processed by the AFM software considering the X and Y position of the probe. All the information collected enable the creation of a three-dimensional image of the sample, and the study of the mechanical properties of the sample [1, 5, 6].

The main parts constituting the atomic force microscope are reported in fig.1.1 and are described in the following paragraphs.

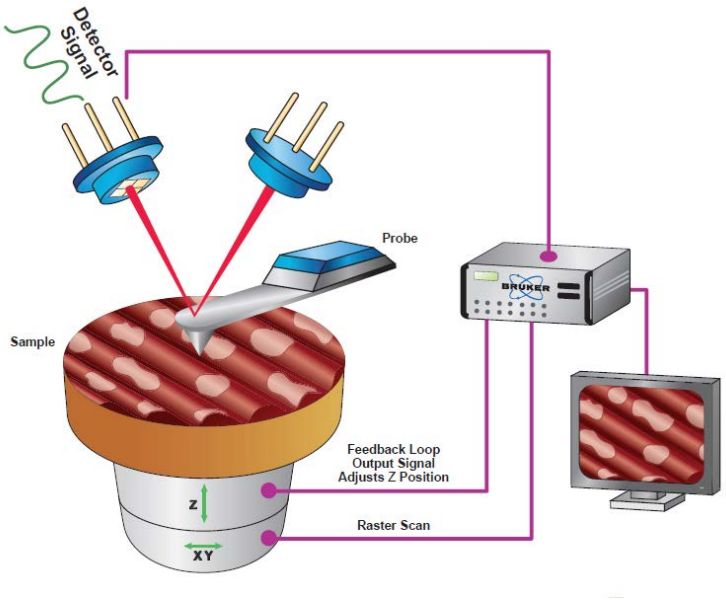

Figure 1.1 – AFM functioning scheme. The main components of the microscope are reported. © Copyright Bruker

1.2 Cantilevers and tips

Cantilevers are usually made with silicon, or its derivates (nitride or oxide), by microfabrication (lithography and etching). They can be coated with metals (e.g. Au) to increase the laser reflection and/or permit their functionalization.

The shape can be triangular (V-shape) or rectangular. Triangular cantilevers are less resistant to vertical deflection than rectangular cantilevers, but they are more resistant to torsion. The dimensions are usually between 100 and 200 μm in length, 15 and 35 μm in width and 0.3 and 2 μm in thickness. These range of sizes permit to obtain cantilevers with different elastic constants and resonance frequencies. Shorter and thicker cantilevers are stiffer and have higher resonance frequencies than longer and thinner cantilevers.

The probe (tip) of the cantilever is the part that directly interacts with the sample. A wide range of geometries is available, spherical and pyramidal are the most commonly used. The radius of curvature influences the spatial resolution, the choice of the geometry therefore depends on the application [7,8].

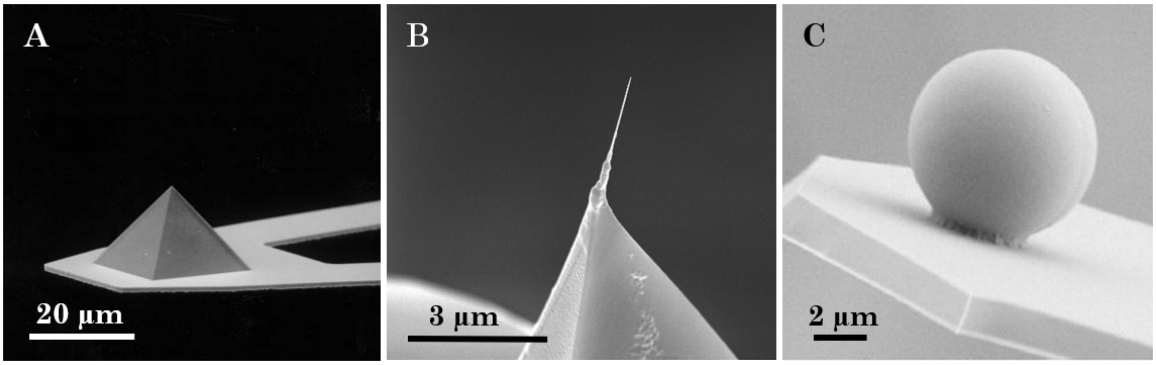

Figure 1.2– Examples of commercial probes. Pyramidal tip (A){Fery, 2004} and ultrasharp tip (B) credits K-Tek Nanotechnology, colloidal probe (C){Niedermann, 1998}.

Normal tips are tips with pyramidal shape, a height of about 3 - 15 μm and a radius of curvature of about 30 nm. Sharp tips are thinner than normal tips and therefore the radius of curvature is smaller. Ultrasharp are tips even more thin and longer with radius of curvature that can arrives to 10 nm. Colloidal tips are obtained attaching a sphere (range between 1 and 50 μm) to the end of the cantilever, usually they are made with gold, silicon oxide or polystyrene [6, 9].

1.3 Sample-probe positioning

The scan is performed using a piezoelectrical system, that can be placed in the head or in the sample holder, depending on the AFM model. Usually the system

consists in a piezoelectrical tube with an inner electrode and four outer electrodes. The variation of potential applied to the electrodes enables the three direction movements (x, y, z) of the system. The piezoelectrical tube is made with materials that expand or contract in presence of a voltage gradient. The application of a potential to the four outer electrodes and the inner electrode leads to the elongation or retraction of the tube (z movement). The application of a potential to two of the outer electrodes causes the elongation of a sector and the retraction of the other one, leading to a movement in the x-y plane. A calibration with microfabricated gratings in the same range of the sample features is required, in order to correct the hysteresis of the piezoelectric actuator.

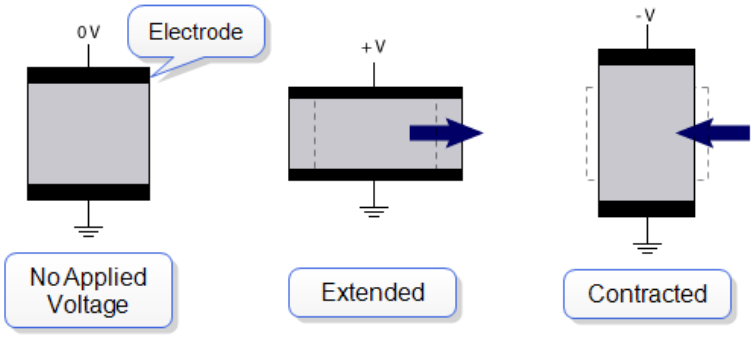

Figure 1.3 – Piezoelectric tube in the case of potential applied.
© Copyright Bruker

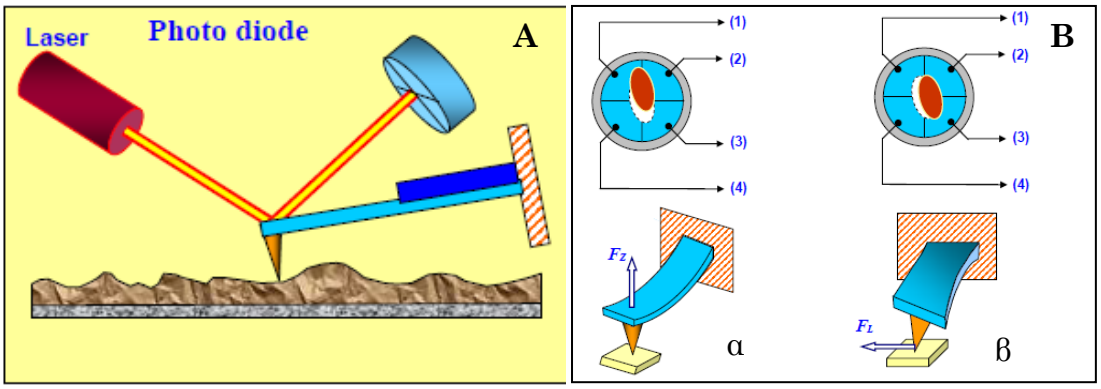

Figure 1.3 – Illustration of the optical system that detect the cantilever deflection (A). Relation between vertical (α) and lateral (β) cantilever bending (bottom) and the respective signal to the photo diode (top). [1]

1.4 Feedback system

As it can be observed in fig. 1.4, a laser is focused on the cantilever and then reflected through a mirror system to a photo diode. The photo-diode usually has four quadrants and it converts the cantilever deflection, due to the interaction with the sample, to an electric signal. Then, a control unit has the role of signal elaboration and regulates the relative vertical distance between the probe and the sample [10].

1.5 Force curves

The AFM enables to collect information about the mechanical properties of the sample through indentation tests that give an approach curve and a withdraw curve (fig. 1.5). The electric signal collected by the photo diode is then converted to force, as follow:

$$F = k \cdot s \cdot \Delta V \tag{1.2}$$

where F is the force measured (N), k is the force constant of the cantilever (N/m), s is the sensitivity of the optical system (m/V) and ΔV is the signal of the photo diode (V) [11].

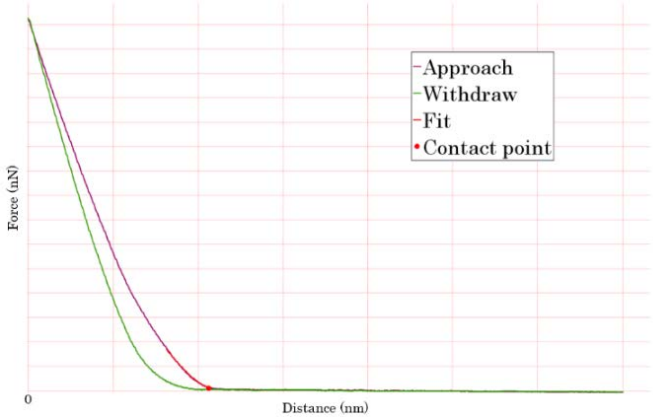

Figure 1.5 – Force – distance curve. The contact point is marked in red.

From the approach curve is possible to obtain the Young's modulus, which is commonly used to describe the stiffness of the sample. For this purpose, curve indentation models must be used for the fitting. Various models are available

based on the specific geometry of the probe (e.g. Hertz, Sneddon). In the case of spherical tips, the Hertz model is one of the most used models, and it has been used for the fitting of the curves presented in the next chapters.

$$F = \frac{4}{3}\frac{E}{1-\nu^2}\sqrt{R\delta^{\frac{3}{2}}} \tag{1.3}$$

where F is the force, from the force curve, E is the Young's modulus, ν is the Poisson's ratio (depending on the sample, usually 0.2 – 0.5), R is the radius of the tip and δ is the indentation [8].

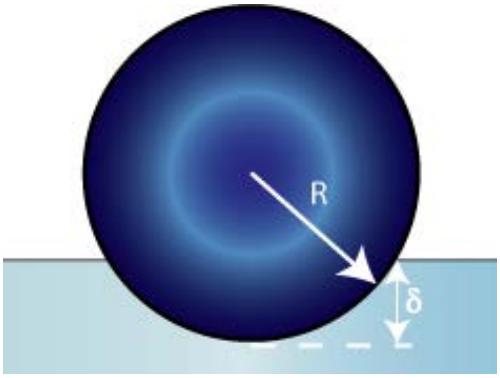

Figure 1.6 – Image of the contact between an elastic half space and a sphere, Credits Bruker.

1.6 Mechanical study of biofilms using the AFM

Force spectroscopy measurements using the AFM can be performed in liquid, and this permits to investigate biological samples that require special operative condition to maintain them "healthy". This working condition allows the investigation of the mechanical properties of bacterial biofilms *in vivo*. The potentials of the use of the AFM to investigate bacterial biofilms are well known in literature. As an example, Safari et al. investigated the mechanical properties of a mature biofilm from a wastewater system with different methods, from macroscale compression to microscale indentation [12]. In another study, Huang et al. showed how the AFM is a valid method to measure the adhesion forces between bacteria and mineral in water [13]. Concerning the effect of disinfection

on biofilms, it is particularly relevant the study conducted by Shen et al. on the use of the AFM to monitor the changes in mechanical properties of a biofilm grown for one year in potable water and then subjected to prolonged chlorine exposure [14]. This study showed that the use of chlorine reduces initially the thickness of the biofilm, which hence tends to become stiffer, while it loses its effectiveness along the second and third month as it is demonstrated that the biofilm regains thickness and elasticity due to the development of resistance to the chlorine.

However, in literature there is a lack of studies relating mechanical properties and biofilm ages, relation that could be crucial to understand the biofilm variations over time. This aspect led to the design of the experiments on the mechanical study of biofilms of different ages, that are presented in the following chapters.

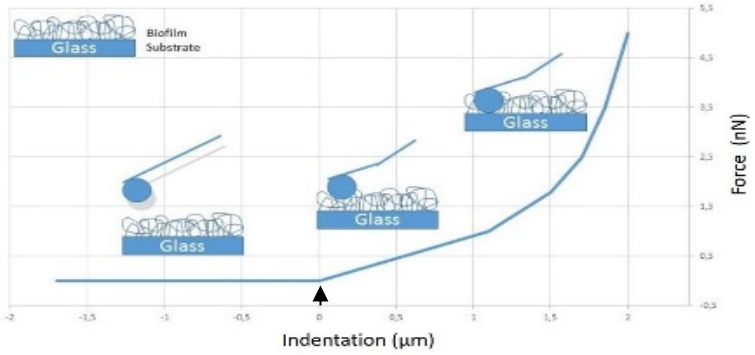

Figure 1.7 – Ideal approach force curve of a biofilm sample. In the first part the tip is not in contact with the sample, after the contact point (black arrow) it starts to indent the biofilm.

1.7 Concluding remarks

Atomic force microscopy is a scanning probe technology that permits to study a wide range of samples, including biological samples. In the following chapters the results of force spectroscopy studies performed using the AFM on bacterial biofilms are reported. Morphological studies were conducted in parallel with the AFM used as imaging tool. Fundamentals of imaging methods and results of imaging studies are presented in Part IV.

Materials and methods

2

In this chapter the materials and methods that have been used for the mechanical study of biofilms of different ages are illustrated.

2.1 Materials

In this study, the Gram-negative strain *P.fluorescens* ATCC 13525, P. aeruginosa (PAO1) and *S.aureus* were used. Mueller Hinton (MH) agar and broth for bacterial culture were purchased from Sigma Aldrich. Glass coupons were obtained from microscope slides (Fisherbrand Superforst) cutting pieces of 1x1 cm using a diamond-tip pen. Plastic and stainless-steel coupons were kindle offered by the Department of AgriFood, Environmental and Animal Science of the University of Udine. Phosphate-buffered saline (PBS) and Acridine orange solution were purchased form Sigma Aldrich. AFM probes were purchased from Nano and More GmbH.

2.2 Bacteria and culturing

The stocks of bacteria were stored at -80°C in glycerol (20%) and used to inoculate Mueller Hinton agar plates. Colonies from the plates were inoculated in 20 ml of Mueller Hinton broth and let grow aerobically while shaken overnight (at 26 °C in the case of *P. fluorescens*, 37 °C in the case of *P. aeruginosa* and *S. aureus*). The optical density at a wavelength of 600nm (OD_{600}) of the overnight culture of bacteria in MH broth was determined using a Helios gamma spectrophotometer (Thermo Scientific).

2.3 Preparation of biofilms on different substrates

Glass, polypropylene and stainless steel (1cmx1cm pieces) were used as substrates to grow the biofilms in static conditions. *P. fluorescens*, *P. aeruginosa* and *S. aureus* were used. The overnight culture of bacteria in MH broth was diluted to obtain an OD_{600}= 0.1 and 2ml of the suspension was used to cover the substrates. The samples were incubated at 26°C. The broth was gently replaced with new sterile broth every 24h using a micropipette. The samples were removed at fixed intervals starting after 2h up to 43 days.

2.4 Confocal laser microscopy (CLSM) observation of biofilms on different substrates

The biofilm samples were fixed for one hour at 60°C and then labelled using a 0.1% Acridine orange solution. The analysis was performed using the Nikon Eclipse C1si at 60x and 40x magnifications. The area acquired was 100µm x100µm. Tests have been done on glass, polypropylene and stainless steel.

2.5 AFM force measurements

2.5.1 Sample preparation

Before the analysis, the samples were removed from the MH broth and gently rinsed using PBS buffer.

2.5.2 Force measurements

The mechanical properties measurements were performed in liquid (PBS buffer) using a Bruker Nanoscope 2™. AFM cantilevers with spherical tip were used (Nano and more CP-CONT-SiO-D-5, Ø = 10.2 µm, cantilever: F 13 kHz - C 0.2 N/m – L 450 µm). The calibration of the cantilever deflection signal was performed by acquiring force vs. piezo-displacement curves on a glass substrate (see details in paragraph 2.1). The spring constant of the cantilevers was taken from manufacturer's specifications.

Random parts of each samples were tested and at least 20 curves per sample were collected at 3µm/sec.

2.5.3 Data processing

For the fitting of the force curves, Nanoscope Analysis 1.8 by Bruker was used. The fitting of the Approach curves was done using the "Linearized model" method and the "Hertz model". As the model is valid for small indentation, as reported in literature, only the 10% of the height of the cell was fitted. The curves collected in empty parts of the sample, easily recognisable as the transition from the non-contact to the contact- part of the curve is very harsh (fig. 2.1 A), were not processed.

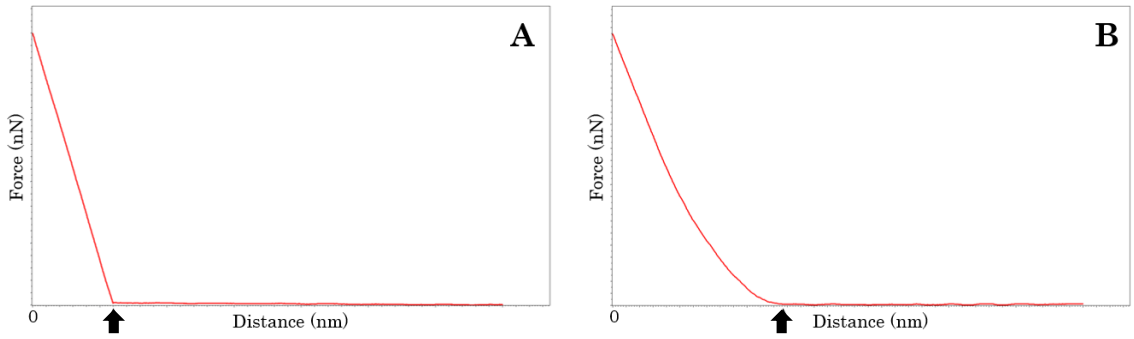

Figure 2.1 – Force curves representative of (A) an empty part of the sample (substrate) and (B) a biofilm portion of the sample. It is possible to observe the different transition between non-contact and contact part of the curves. The points of transition are highlighted by a black arrow.

2.5.3.1 Cell- height measurement

In order to determine the height of the cell, and consequently the indentation depth to fit, images of *P.fluorescens* cells *in vivo* in liquid were acquired in peak force mode using a Bruker BioScope Resolve™ BioAFM.

2.6 Acknowledgments

This study has been performed in collaboration with Biophyna team at LOMA laboratories (Laboratoire Ondes et Matière d'Aquitaine), Bordeaux, France.

Results and discussion

3

In this chapter the results of the mechanical study on biofilm of different ages are presented and discussed. From collected data it appears that the distribution of the Young's modulus in the different areas of the biofilm is related to the age of the biofilm. A possible explanation of the phenomenon is proposed.

3.1 Preliminary study of the influence of the substrate in biofilm formation

In order to choose the substrate for the mechanical investigation of biofilms of different ages, a preliminary study of the effect of substrates on biofilm formation was performed.
Glass, polypropylene and stainless steel were tested as potential substrates. *P.fluorescens*, *P.aeruginosa* and *S.aureus* were used to grow biofilms on these substrates from 1 day up to 10 days.
The growth of bacterial biofilms depends on various conditions, the substrate is a condition that has a relevant role in this process, as it is possible to observe in the following CLSM images.

In fig. 3.1, 3 days old *P.fluorescens* biofilms on glass and on stainless-steel are reported. It is evident that even if the two biofilms grew up under the same conditions, there are less cells attached to the stainless-steel compare to the glass substrate.

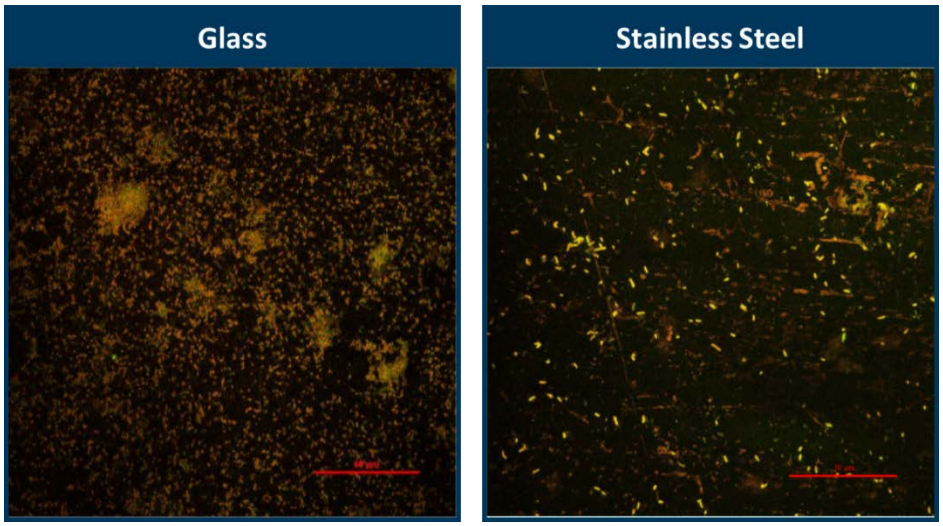

Figure 3.1 – CLSM images of P. fluorescens 3 days old biofilms on glass (A) and stainless-steel (B).

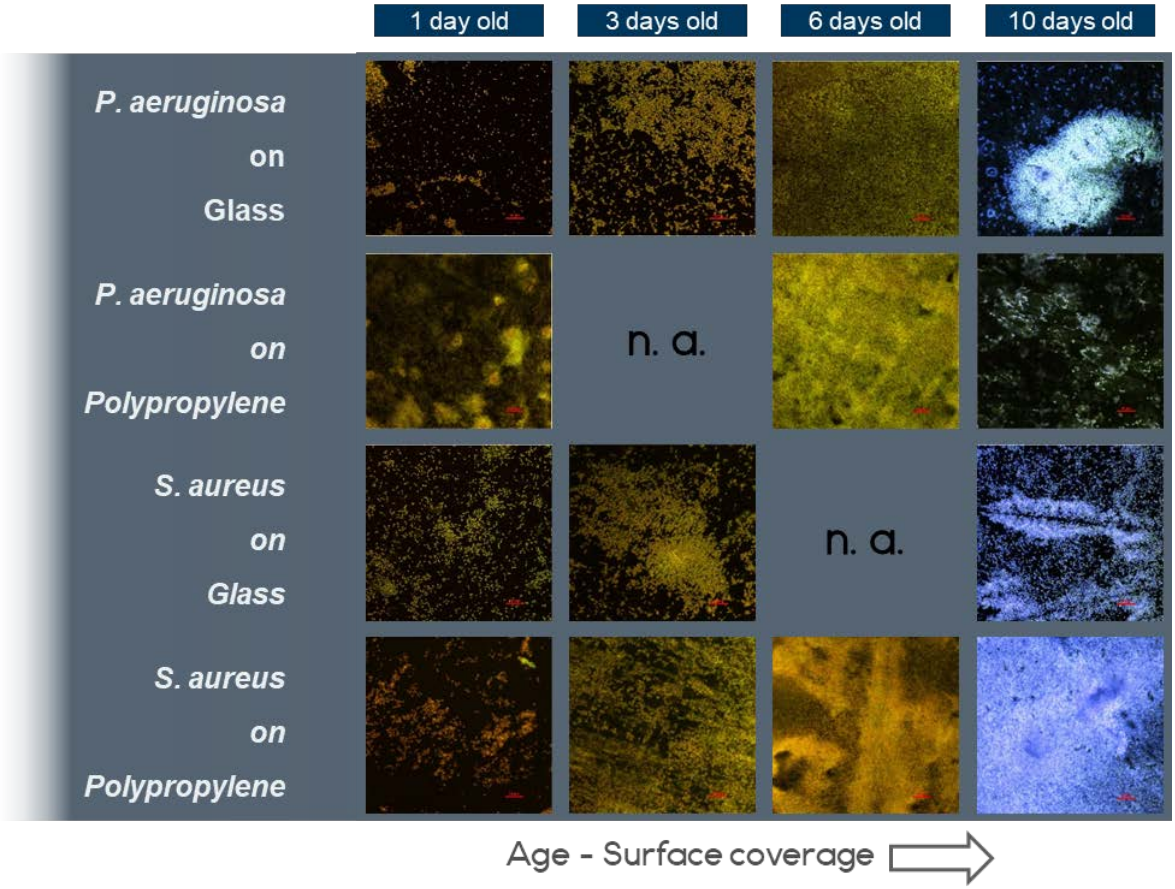

Figure 3.2 – CLSM images of biofilms of different ages on glass and polypropylene substrates. The images collected show a relation between age and surface coverage for both P. aeruginosa and S. aureus.

It appears that stainless-steel is not a good substrate for the growth of bacterial biofilms, this is probably due to its composition, and this is one of the reasons why it is widely used in food industry.
Stainless steel does not favour the development of biofilms, on the other hand both glass and polypropylene substrates have proven to be good substrates (fig. 3.2).

Glass coupons have been chosen for the following experiments because of the good performances during the preliminary study, and also because glass is transparent, and this property makes it a good material for the sample visualization during AFM experiments.

3.2 Mechanical study of bacterial biofilms - Samples

The AFM was used to measure the mechanical properties of biofilm of different ages on a glass substrate. After many tests to optimize the experiments, more than 400 curves were collected from biofilm of different ages, starting from 7 days up to 43 days (table 3.1).

Since biofilms are heterogeneous structures, every sample shows areas (regions) with different mechanical properties [14]. These areas could be classified considering the Young's modulus (E) from which they are characterized, as reported in table 3.2. Thereafter the Young's modulus-area will be indicated with the acronym (YMA).

Table 3.1 - Biofilm samples collected

Bacterial Strain	Biofilm samples (at least 3 repetitions each)
P. fluorescens (ATCC 13525)	7 days old
	20 days old
	29 days old
	36 days old
	43 days old

Table 3.2- Young's modulus-areas (YMA)

Areas	Young modulus
Very soft areas	E <5 kPa
Soft areas	5 kPa< E <30 kPa
Hard areas	30 kPa< E<100 kPa
Very hard areas)	E >100 kPa

In this study, at least 20 random sites of each sample were analysed using the AFM obtaining their Young's modulus. It was possible to observe how the

Elastic modulus values of a biofilm of a certain age are distributed among the different YMA and compare this data with the data form older and younger biofilms.

3.3 Data analysis

3.3.1 In vivo measurement of the size of P. fluorescens cell

As anticipated in *Materials and Methods*, the fitting models are valid for small indentations and, from literature, just the 10% of the height of the cell must be fitted. For this reason, it is important to determine the size of the cell. Images *in vivo* in liquid of *P. fluorescens* cells were collected. The average height of the cells resulted 652 nm (st.dev. 22.68).

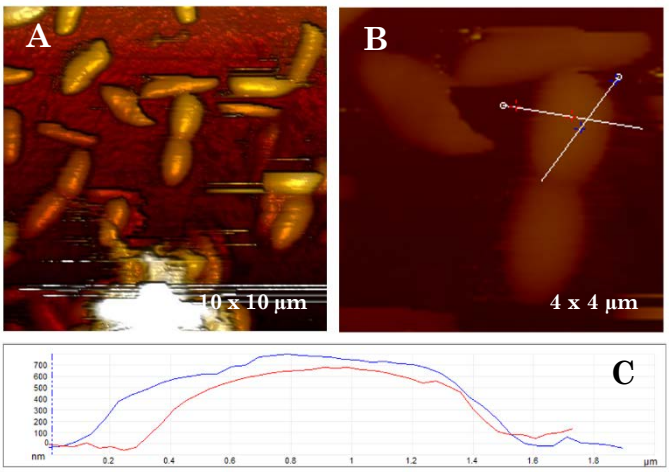

Figure 3.3 - AFM height images in vivo in liquid of *P.fluorescens* (A, B) with cross section (C).

3.3.2 Data analysis and statistics

The force curves collected were fitted applying the Hertz model:

$$F = \frac{4}{3}\frac{E}{1-\nu^2}\sqrt{R\delta^{\frac{3}{2}}} \tag{3.1}$$

where F is the force, from the force curve, E is the Young's modulus, ν is the Poisson's ratio (depending on the sample, usually 0.2 – 0.5), R is the radius of the tip and δ is the indentation.

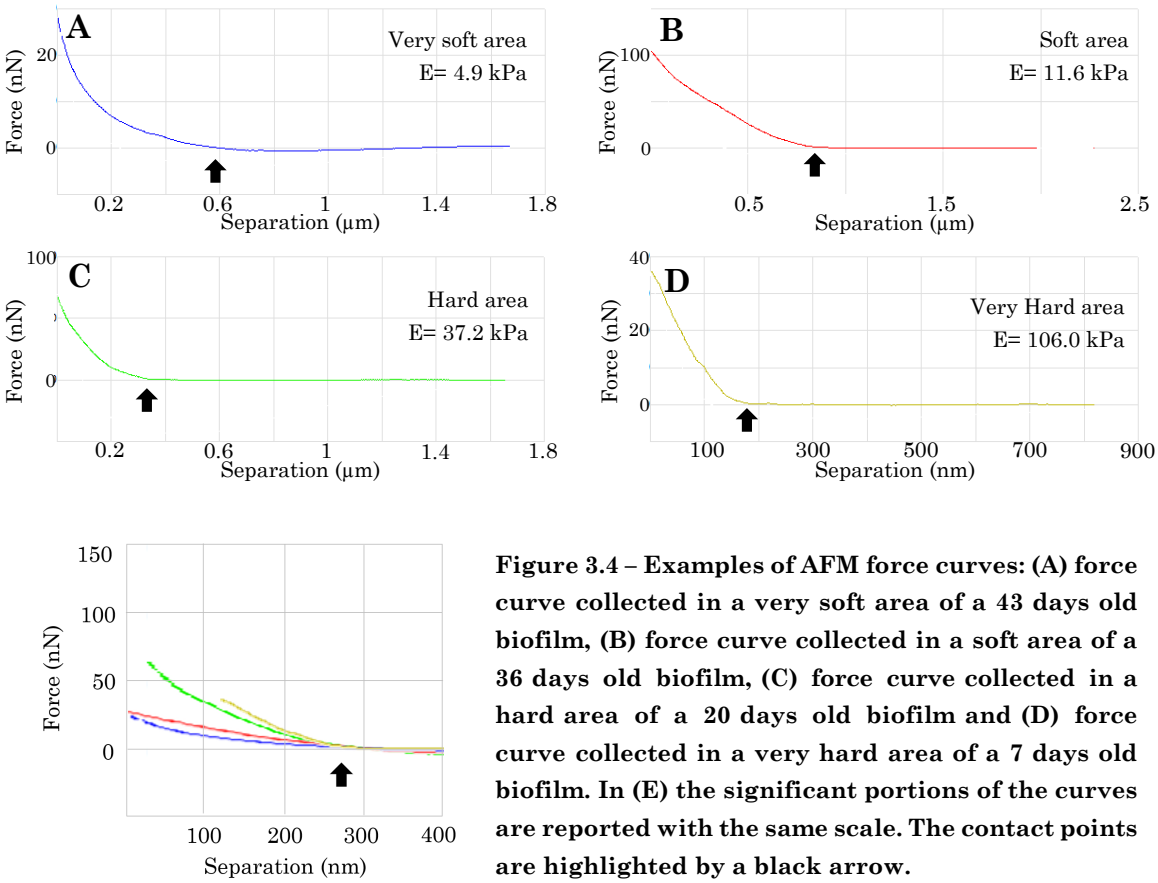

Figure 3.4 – Examples of AFM force curves: (A) force curve collected in a very soft area of a 43 days old biofilm, (B) force curve collected in a soft area of a 36 days old biofilm, (C) force curve collected in a hard area of a 20 days old biofilm and (D) force curve collected in a very hard area of a 7 days old biofilm. In (E) the significant portions of the curves are reported with the same scale. The contact points are highlighted by a black arrow.

In fig. 3.5 the graphs of the samples are reported. It is possible to observe that every sample follows a gaussian-like dispersion function (bell function). The bell varies from height, width and position and it shifts from the very hard- to the very soft- area. It is also possible to observe that the data are more spread in the samples of intermediate ages.

The graphs reported in fig. 3.6 show the different trends from 7 to 43 days. These graphs give the same information showed in those in fig. 3.5, describing the data summarized by areas instead of by age. In the case of the very soft and soft areas, it is possible to observe that the trend shows that the older is the sample, the softer is the sample. For hard and very hard areas, the trend shows an opposite behaviour. It is going down slowly: the older is the sample, the harder is the sample.

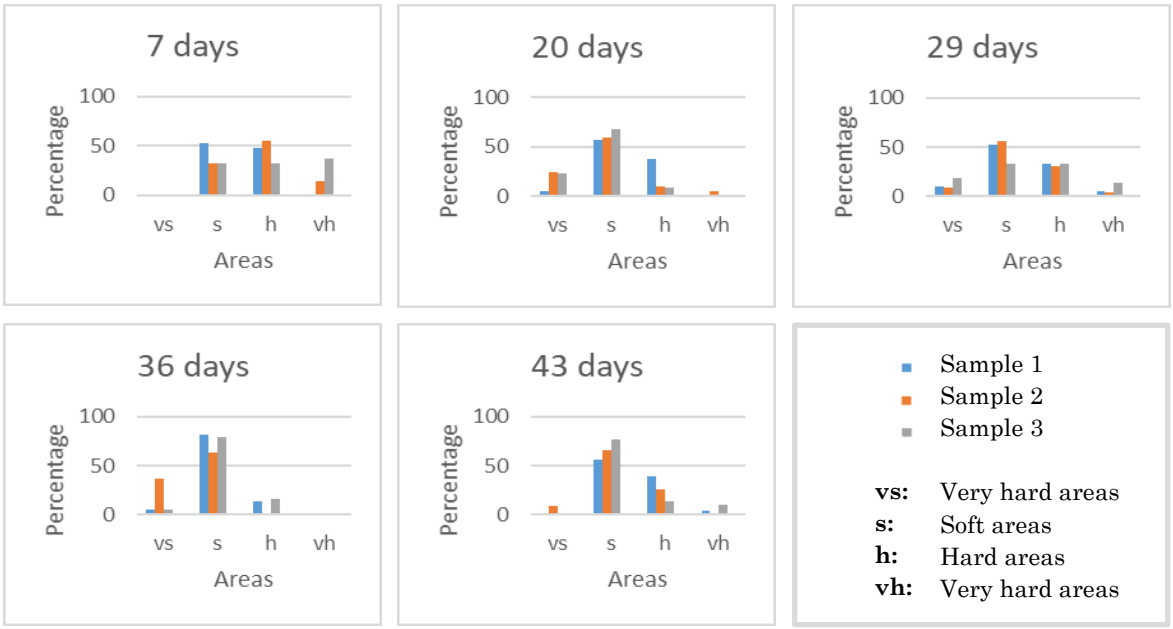

Figure 3.5- Graphs showing the distribution of the Young's modulus among the different YMA. The data are grouped by age of the sample. The three repetitions of the experiment (sample 1, sample 2, sample 3) are reported separately.

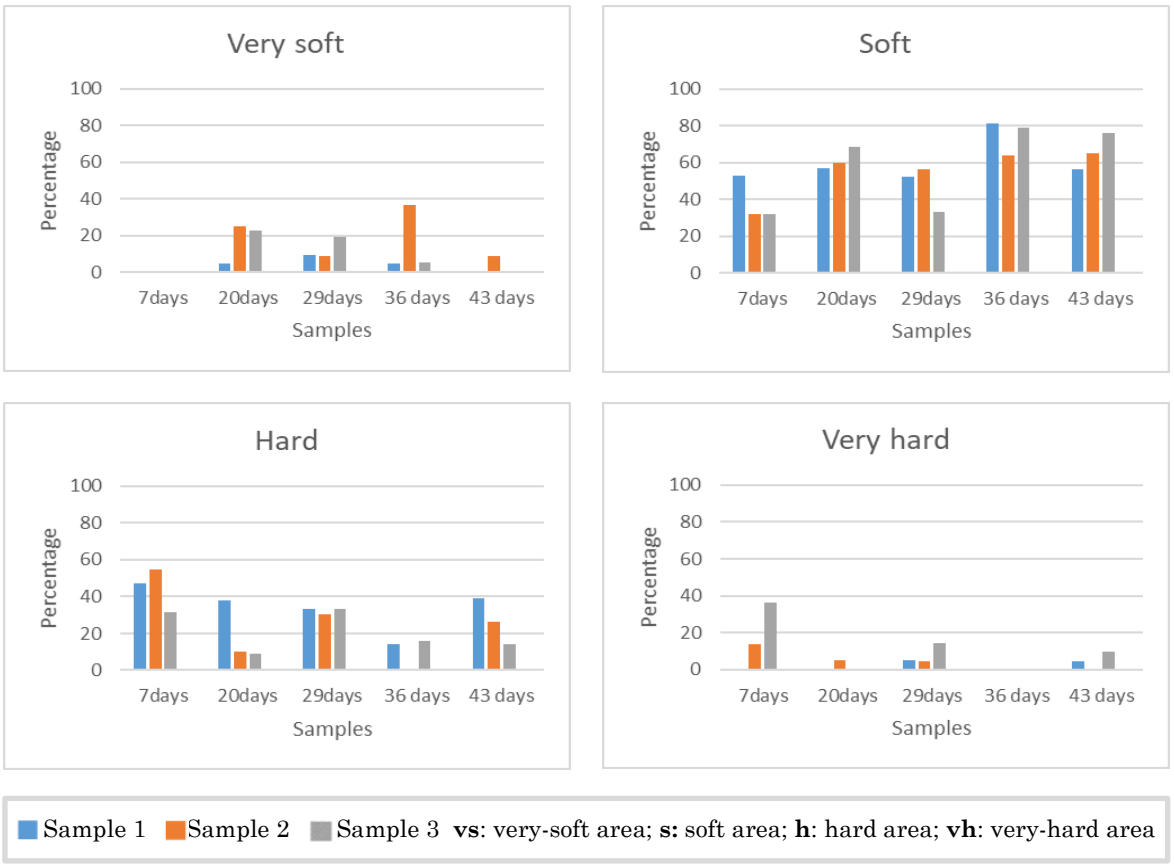

Figure 3.6 - Graphs showing the distribution of the Young's modulus among the different YMA. The data are grouped by YMA. The three repetitions of the experiment (sample 1, sample 2, sample 3) are reported separately.

The data collected showed a phenomenon that can be described in fig. 3.7. The distribution of the Young's modulus in the different areas appears to be related to the age of the samples, starting with a distribution more centred in the hard YMA for the younger samples, that moves to the soft YMA for older samples.
The phenomenon that has been observed could appear peculiar, but an explanation directly related to the structure of the biofilm may be possible.

As reported in Part I – Chapter 1, a biofilm is a very complex and heterogeneous structure characterized by aggregates of bacteria that can give to the biofilm a mushrooms-like shape (fig. 3.8). A "mushroom" is characterized by multi-layers of bacteria, one on the other one that appear softer to the AFM probe that is pushing on the top of a multi-layers of cells. On the other hand, the measure of a single layer of bacteria on a surface is characterized by the exclusive contribution of the single layer, that is harder than a multi-layer.

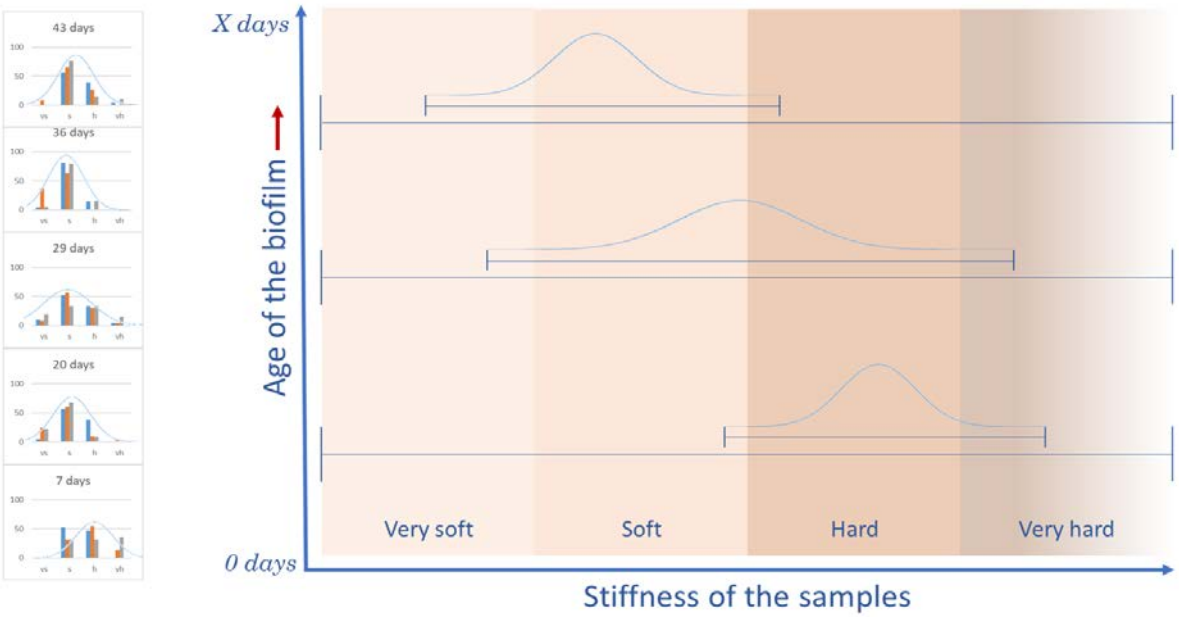

Figure 3.7 – Distribution of the Young modulus in the different YMA of the sample. The distribution is more centred in the hard area for the younger samples and moves to the soft area for older samples.

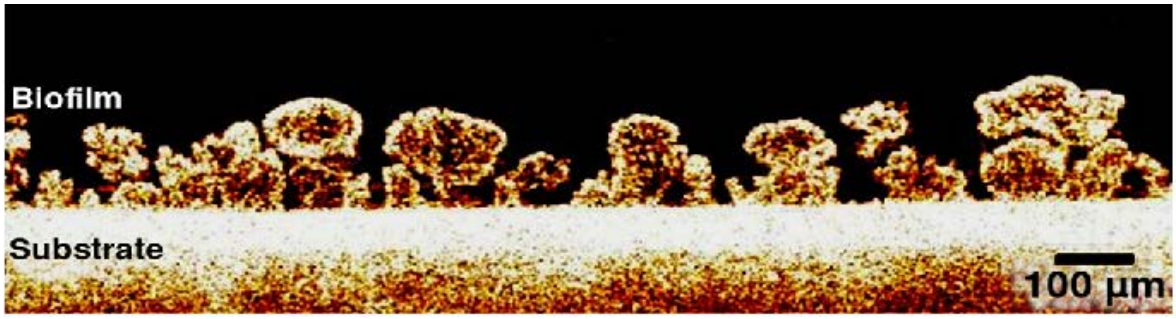

Figure 3.8– Optical coherence tomography (OCT) image of mushroom-like structure of a biofilm (credit Elsevier) [2]

As it was possible to observe during the CLSM study of biofilms of different ages, there is a correlation between surface coverage and age. Studying younger biofilms, there is a high probability that the tip of the AFM randomly arrives in contact with a mono-layer of bacteria. Studying an older biofilm there is a higher probability that the tip randomly arrives on the top of a "mushroom", as the surface coverage is higher compare to younger biofilms.

Conclusions and perspectives

4

In this chapter the conclusions derived from the mechanical study of bacteria biofilms of different ages are reported. Perspectives to further development of the study are proposed.

4.1 Conclusions

The investigation of bacterial biofilms of different ages using the AFM allowed to observe that the distribution of the elastic modulus in the various YMA depends on the age of the sample. The distribution follows a Gaussian function that is more centred in the hard area for the younger samples and tends to shift to the soft area for older samples. This behaviour may be explained considering the heterogeneous nature of the biofilm.

4.2 Perspectives

A possible explanation of the phenomenon observed has been proposed, other experiments are necessary to validate it. In particular, it is necessary to perform the same tests on biofilm of other strains, both Gram-positive and Gram-negative bacteria. Investigating new samples, it will be possible to understand if the phenomenon is common to different species or if it is specific of *P.fluorescens*. Another important step would be the investigation of multi-species biofilms.

In this study, samples from 7 days up to 43 days were tested. It would be interesting to observe how the elastic properties are distributed in the different YMA in the case of older biofilms.

The biofilms used for this study grew in optimal condition (optimal growth temperature, nutrients available…), which are not the condition commonly available in nature. The development of a biofilm is influenced by the environmental conditions and this could lead to different properties of the biofilm itself (for example, the quantity of extracellular matrix produced). Interesting observation could be done comparing the data collected changing one parameter each time (nutrients availability, presence of a flow…).

In this study, the Young modulus of bacterial biofilms has been investigated. A complementary study would be the examination of the adhesion properties of the biofilms, in order to observe if there is a correlation between adhesion properties and age of the biofilm, as observed in the case of mechanical properties.

References

5

1. Mironov, V.L., *Fundamentals of scanning probe microscopy*, ed. T.r.a.o.s.i.f.p.o. microstructures. 2004: NT-MDT.
2. Fischer, M., G.J. Triggs, and T.F. Krauss, *Optical Sensing of Microbial Life on Surfaces.* Applied and Environmental Microbiology, 2016. **82**(5): p. 1362-1371.
3. Binnig, G., C.F. Quate, and C. Gerber, *Atomic Force Microscope.* Physical Review Letters, 1986. **56**(9): p. 930-933.
4. *BASIC PRINCIPLES*, in *Atomic Force Microscopy for Biologists*. p. 44-75.
5. Meyer, G. and N.M. Amer, *Novel optical approach to atomic force microscopy.* Applied Physics Letters, 1988. **53**(12): p. 1045-1047.
6. *APPARATUS*, in *Atomic Force Microscopy for Biologists*. p. 5-43.
7. *http://www.ntmdt-tips.com/*.
8. *https://www.brukersupport.com/*.
9. Albrecht, T.R., et al., *Microfabrication of cantilever styli for the atomic force microscope.* Journal of Vacuum Science & Technology A, 1990. **8**(4): p. 3386-3396.
10. Baselt, D.R., et al., *Digital signal processor control of scanned probe microscopes.* Review of Scientific Instruments, 1993. **64**(7): p. 1874-1882.
11. Morris, V.J.A.K., A R%A Gunning, A P, *Atomic Force Microscopy for Biologists*. Atomic Force Microscopy for Biologists.
12. Safari, A., et al., *Mechanical properties of a mature biofilm from a wastewater system: from microscale to macroscale level.* Biofouling, 2015. **31**(8): p. 651-64.
13. Huang, Q., et al., *Atomic force microscopy measurements of bacterial adhesion and biofilm formation onto clay-sized particles.* Sci Rep, 2015. **5**: p. 16857.
14. Shen, Y., et al., *Response of Simulated Drinking Water Biofilm Mechanical and Structural Properties to Long-Term Disinfectant Exposure.* Environmental science & technology, 2016. **50**(4): p. 1779-1787.

Part III

Real-time monitoring of biofilm growth and disinfection

The quartz crystal microbalance with dissipation module

1

The development of a sensor able to detect in real time the presence of a biofilm in early stages of growth, and the effect of disinfection, is a requirement because of the threat that the presence of bacterial structure represent in many fields, from hospital to daily life.

A sensing system capable of detecting biofilms across a range of applications implies that it must be based on a transducer that sense general properties of a biofilm like the mass, the density, the stiffness, the electrical impedance, etc.
In this regard, the AFM study, presented in Part II, allowed us to study the mechanical properties of biofilms over the time. With this know-how, research moved to a highly sensitive, robust and compact device, that permits the monitoring of mass and viscoelastic properties variation in real-time: the quartz crystal microbalance (QCM) with dissipation module.
Using a QCM, it is possible to study many types of samples, bacterial biofilms included, due to the sensibility of the technique measuring small mass changes in a particular environment. In this way, it is possible to study living cells on a surface both during the adhesion process and the growth.

In this chapter, the principles of the quartz crystal microbalance technology are presented. In addition, the application of this technology for the investigation of bacterial biofilms is illustrated.

1.1 The sensor

The sensor used in the QCM is a piezoelectric quartz crystal. In order to permit to the acoustic wave to propagate perpendicularly to the crystal surface, the quartz plate must be cut in a specific way defined by the crystal axes (fig. 1.1 A-B). AT- cut quartz is the most used because, as the temperature coefficient at room temperature is low, small changes in temperature involve small changes in frequency. Each side of the quartz is coated with a gold electrode (fig. 1.1 C) [1, 3].
When an alternating voltage is applied, the quartz sensor oscillates (fig. 1.2). Every quartz has its characteristic resonance or fundamental frequency (fig. 1.3) that is given by the following equation:

$$f_0 = \sqrt{\frac{\mu_q}{\rho_q}} / 2t_q \qquad (1.1)$$

where μ_q is the shear modulus of the quartz, ρ_q is the density of the quartz and t_q is the crystal thickness.

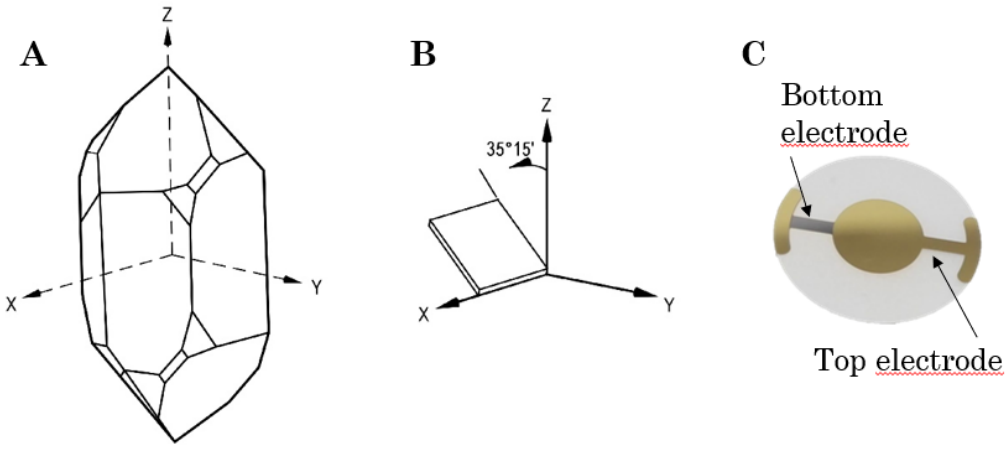

Figure 1.1 – Axes of a quartz crystal (A); AT-cut quartz crystal (B); commercial AT-cut gold quartz (C) [3]

The oscillation frequency is influenced by some constant factors, like quartz thickness (a thinner quartz has a higher oscillation frequency and sensitiveness), density and shear modulus, and by some properties of the media

(liquid or air) in contact with the quartz and of the deposited layers, such density or viscosity [1, 3].

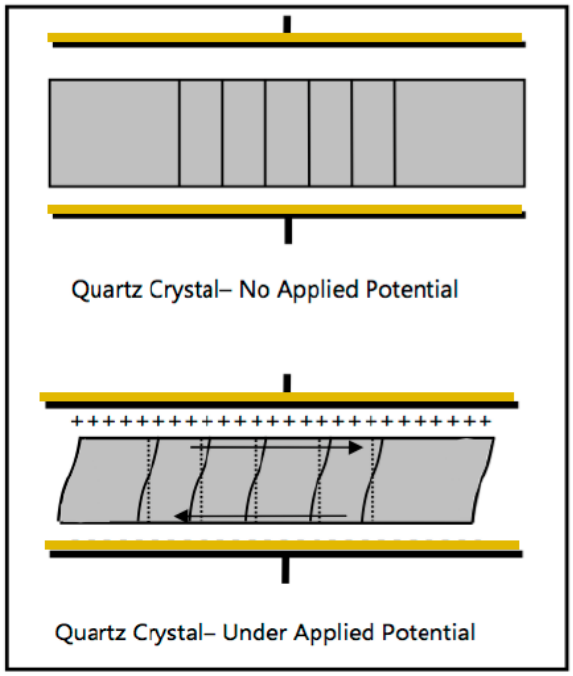

Figure 1.2 - Thickness shear deformation of the quartz [1]

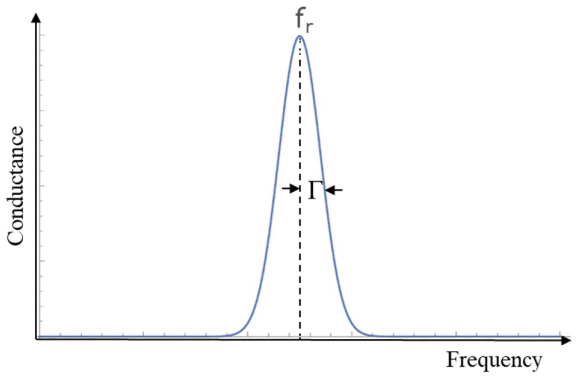

Figure 1.3 - Resonance frequency of the quartz

1.2 Interpretation of the signals

Information are obtained observing the shift in the frequency of oscillation of the quartz due to the deposition of a sample on its surface. A frequency shift and, additionally, a damping of the oscillation occur when a deposition on the

quartz surface is happening. A QCM with a dissipation module can capture both the variation in frequency and in the dissipation of the energy.

The relation between dissipation (D) and damping (Γ) is define as reported in equation 1.2, where D is the dissipation, Γ is the half width at half maximum and f_r is the resonance frequency of the crystal.

$$D = 2\Gamma / f_r \tag{1.2}$$

Depending on the characteristics of the samples, there are some equations that can be used for the interpretation of the signals, as reported in the following paragraphs.

1.2.1 Rigid layer in gas phase

In the case of a rigid layer in gas phase, the damping parameter is often negligible and the mass change on the sensor can be determined using the Sauerbrey's equation:

$$\Delta f_{Sauerbrey} = -C\,\Delta m \tag{1.2}$$

This equation put in relation the resonant frequency shift (Δf) and the mass shift (Δm) of the film deposited on the surface of the quartz; C is a constant related to the properties of the quartz (thickness, density, resonance frequency, surface area). However, this equation is usable for films that are rigid, thin and homogeneous. The frequency-mass correlation of depositions that don't satisfy any of these conditions are more complicated. [2, 4]

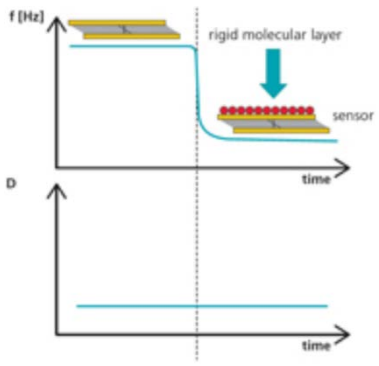

Figure 1.4 - Ideal signal in the case of rigid layer in gas phase [2]

1.2.2 Liquid phase analysis

When the surface of the sensor is completely covered by a fluid, there is a damping in the oscillation of the quartz and, because of this, the energy loss increases. In these conditions, it is possible to observe a change in frequency and in the damping parameter that is related to the properties of the fluid.
In the case of Newtonian fluids, the introduction of a fluid with higher viscosity and density will lead to a decrease in frequency and an increase in damping with an equal amplitude, as defined by the equation of Kanazawa[2]:

$$\Delta f_{Kanazawa} = -\Delta\Gamma_{Kanazawa} \tag{1.3}$$

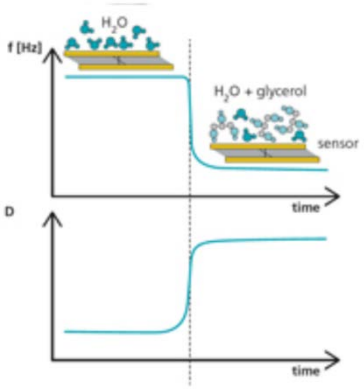

Figure 1.5 - Ideal signal in the case of liquid phase analysis[2]

1.2.3 Rigid layer in liquid phase

In this case, density and thickness determine the layer. The two cases explained in the previous two paragraphs combine[2]:

$$\Delta f = \Delta f_{Sauerbrey} + \Delta f_{Kanazawa} \text{ and } \Delta\Gamma = \Delta\Gamma_{Kanazawa} \tag{1.4}$$

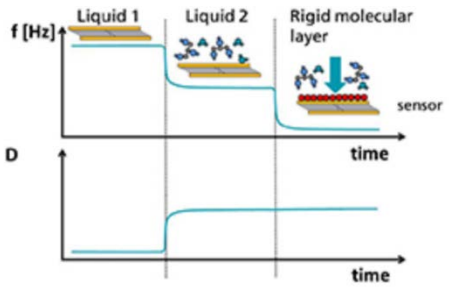

Figure 1.6 - Ideal signal in the case of rigid layer in liquid phase[2]

1.2.4 Viscoelastic layer in liquid phase

In the case of a viscoelastic layer covered with liquid, such as a bacterial biofilm, the damping is no more neglectable. A viscoelastic film, in fact, will not couple fully the oscillation of the quartz and will cause a relevant damping.
The dissipation (D) of the oscillation of the crystal represents the softness of the sample. [4] Differently from Newtonian fluids, f and Γ change in opposite direction, but with different amplitudes.[2]

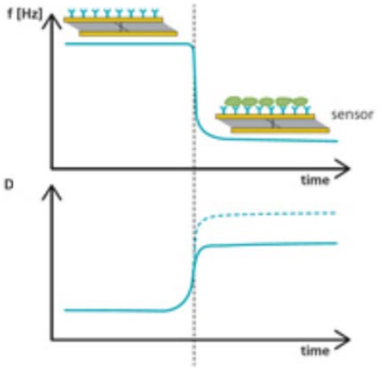

Figure 1.7 -- Ideal signal in the case of viscoelastic layer in liquid phase [2]

Energy dissipation mainly occurs when the structure is porous and viscoelastic and is stretched during oscillation, and if there is trapped liquid that moves in the pores because of the film deformation. All the factors that contribute to the viscoelastic load, and then to energy dissipation, are not fully separable. [4, 5]

1.3 The use of QCM for the real-time monitoring of biofilm formation and disinfection

Bacterial biofilms are viscoelastic porous structures with properties that overlap with those described in the previous paragraphs.
The development of a biofilm on QCM crystal surface results in the decreasing of the frequency, due to the mass increasing on the quartz, and in an increasing of the dissipation of the energy due to the increased viscoelasticity of the sample. Bacteria that form a biofilm, in fact, produce the extracellular polysaccharide matrix (EPS) that is mainly composed by water and polysaccharides [6, 7]. As observed by Schofield et al. using *S. mutans*, the larger dissipation that is possible to observe in the presence of bacteria may reflect EPS matrix

production because of the presence of the cells and the subsequent development of the biofilm [4].

By measuring the frequency and the dissipation, it is hence possible to monitor in real-time the formation of the biofilm on the surface of the sensor. If a disinfectant is introduced in the system, it is possible to follow simultaneously the variations of the mass and of the mechanical, by recording the changes in frequency and dissipation.

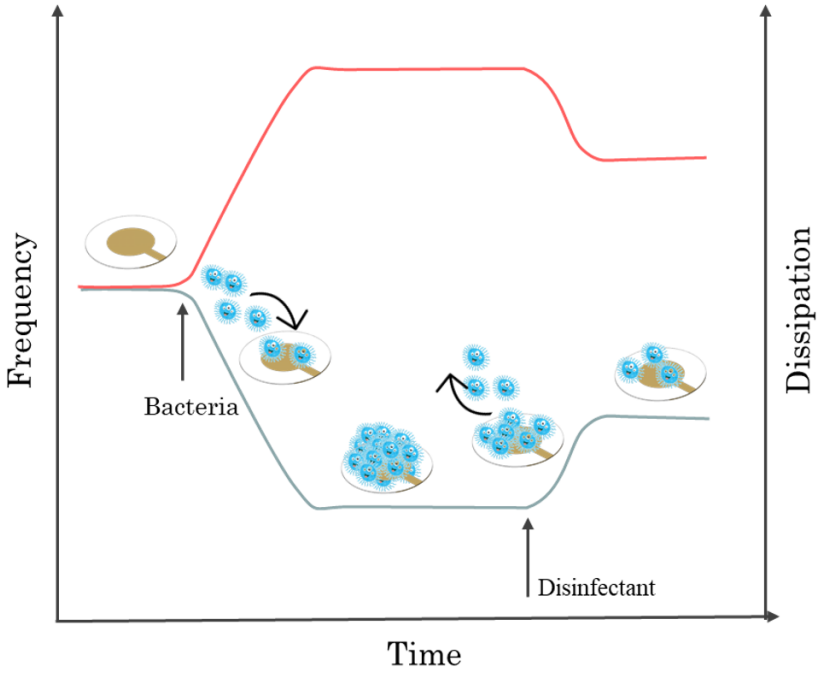

Figure 1.8 – Illustration of the ideal signal that is possible to obtain performing QCM+ dissipation studies on bacterial biofilms. Starting with a signal that is given by the empty quartz covered by culture broth, it is possible to follow the biofilm growth on the quartz and the bactericidal activity of a disinfectant, as variations in frequency and dissipation.

1.4 Concluding remarks

The objective of this study was to assess feasibility, operational conditions and requirements of a real-time biofilm monitoring system based on a QCM equipped with a dissipation module. This system enabled also to observe the response of the biofilm to a disinfection treatment in terms of biofilm mass and viscoelastic properties changes, associated to variations of the oscillation frequency (Δf) of the quartz and of the dissipation energy (ΔD) respectively.

Materials and methods

2

In this chapter the materials and methods that have been used for the real-time monitoring of biofilm growth and disinfection are illustrated.

2.1 Materials

In this study, the Gram-negative strain *E. coli* DH5α was used. Mueller Hinton (MH) agar and Mueller Hinton broth for bacterial culture were purchased from Sigma Aldrich.
Open QCM^{-1} and 10 MHz gold AT-cut quartz crystals were purchased from Novaetech Srl.
Disposable 3-way stop cocks were purchased from Rays, and tubes were purchased from Saint-Gobain and Delta Med.
Amuchina concentrated solution was purchased from Angelini, while Aniosept Active from Anios.

2.2 Bacteria and culturing

The stock of bacteria was stored at -80°C in glycerol 20% and used to inoculate Mueller Hinton agar plates. Colonies from the plates were inoculated in 20 ml of MH broth and let grow aerobically shaken at 37 °C.
The OD_{600} of the culture was determined using using a Helios gamma spectrophotometer (Thermo Scientific) at a wavelength of 600nm and then diluted to OD_{600}=0.2.

2.3 Setup and experiment design

The experiments were performed in liquid by growing the biofilm on a 10 MHz gold AT-cut quartz placed in the chamber of an Open QCM-1. The QCM was placed in an incubator at 36 °C. A peristaltic pump (Masterflex), located after the chamber, was used to pull the liquid through the circuit. The switch between buffer and samples was performed by using 3-way stop cocks (fig. 2.1). Prior to the experiments, both the quartz tuning and the temperature stabilisation have been carried out. As the signal is strongly dependent on the temperature, and the instrument does not compensate it automatically, the thermalisation process has to take place before starting each measurement.

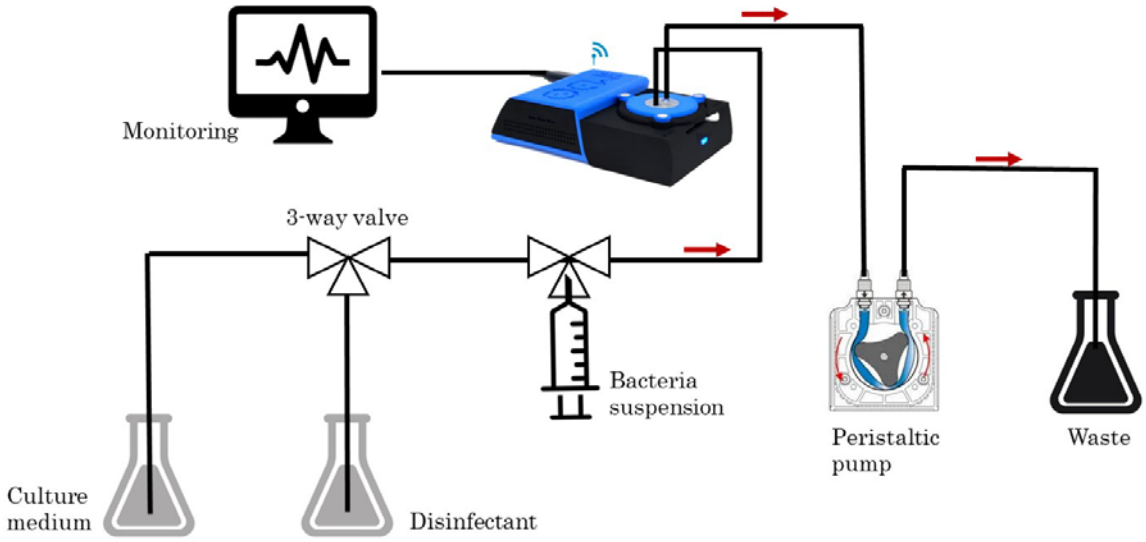

Figure 2.1 – Setup of the experiments.

Figure 2.2 – OpenQCM-1 by Novaetech srl

Two methods were applied: Stop&Go method (that couples static and flow conditions) and the Attach&Flow method (that provides nutrients in a continuous flow). Both methods were characterized by a calibration phase in which the signal in presence of sterile broth was acquired as blank of the experiment.

2.3.1 Real-time monitoring of biofilm growth

2.3.1.1 Stop&Go method

After the stabilization of the signal in static presence of sterile medium (MH broth), the chamber was filled with the suspension of *E. coli* (OD600=0.2) and left in static condition overnight.
The experiment was left in static condition to permit the attachment of bacteria to the surface of the quartz until the next day. In order to provide the nutrients for the growth of the biofilm, at the beginning of each day, the medium was replaced by pumping fresh broth through the chamber for 1 hour at a flow rate of 1mL/h (flow phase). Each flow phase was then followed by a static phase.

2.3.1.2 Attach&Flow method

After the stabilization of the signal in the presence of a flow of sterile MH broth (200µl/h), the bacterial suspension (OD600=0.2) was pumped until the complete replacement of the liquid in the chamber. After 2h in static condition to permit the attachment of bacteria to the surface of the quartz, a 200µl/h flow of sterile broth was pumped into the chamber for 4 days.

2.3.2 Real-time monitoring of biofilm growth and disinfection

2.3.2.1 Stop&Go method

For the real-time investigation of biofilm growth and disinfection, 3 days long-Stop&Go experiments were designed. Two days of growth of the biofilm on the surface of the quartz in MH broth were followed by one day of disinfection. The disinfectant (table 2.1) was pumped into the chamber (flow rate 1ml/h) and let operate in static conditions. At the end of the disinfection phase, sterile broth was pumped into the chamber.

Table 2.1 – Disinfectant compounds and concentrations applied to the experiments.

Disinfectant	Concentration
Amuchina (Sodium Hypochlorite)	0.45% in PBS (50ppm of Sodium Hypochlorite)
	0.9% in PBS (100ppm of Sodium Hypochlorite)
Aniosept Activ (Peracetic acid production in solution)	1% in MilliQ

2.4 Data analysis

The data were acquired using Open QCM^{-1} software, that is an open source Python software.

Results and discussion

3

In this chapter the results of the real-time monitoring of biofilm growth and disinfection are presented and discussed.

3.1 Real-time monitoring of biofilm growth

As mentioned in the section of materials and methods, two different approaches were applied for the monitoring of biofilm growth: a hybrid static + flow method (Stop&Go) and a flow method (Attach&Flow). Traces obtained from various experiments have been analysed in order to extract frequency and dissipation changes characterising the growth of the biofilm and the disinfection effects. A set of examples were selected for discussion as representative of the observed phenomena.

3.1.1 Stop&Go method

In fig. 3.1, frequency and dissipation associated to the growth of *E.coli* biofilm monitored over 6 days are reported.
It is possible to observe that the daily flow phase carried out to provide fresh nutrients to the biofilm removes some material from the quartz surface as shown by frequency peaks after injections. This phenomenon is decreasing day-by-day likely due to a higher stability of the biofilm and the consequent resistance to the stress induced by the flow. A trend is given by the frequency decrease which happens every day showing that the mass on quartz is progressively increasing.
However, it can be noticed that the decrease in frequency recorded over a day is faster at the beginning and tend to reach a plateau towards the end of the day.

In parallel, the dissipation increases initially and reaches a plateau towards the end of each day. In particular, from day 4 we can notice that the dissipation tends to reach a maximum and then decrease slightly towards the end of the day.

The increase in dissipation means a softer deposit. Day-by-day the dissipation of the biofilm decreases signalling an overall hardening of the biofilm. This is likely due to the process of biofilm growth in terms of balance between dead and live cells, and uniformity across the sensing surface. By bearing in mind that the first layers above the sensor surface are dominant in determining the QCM signal, it can be hypothesised that a more mature biofilm causes a lower relative change in frequency while the dissipation sees mainly the inner layer of the biofilm (that has more dead and rigid cells).

The overall behaviour in frequency from day 1 to day 6 seems to indicate that the biofilm system is reaching a regime in terms of development, and this behaviour is probably related to the experimental conditions.

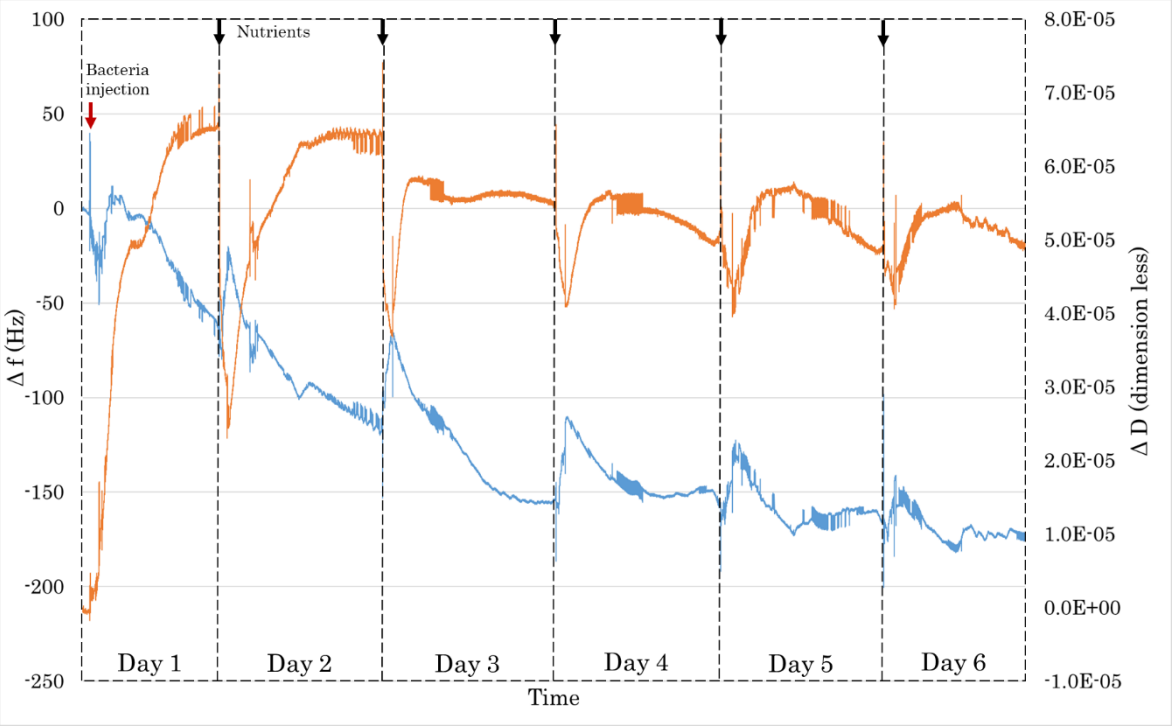

Figure 3.1 – Experiment performed using the Stop&Go method. The frequency is reported in blue and the dissipation in orange. The sample injection is signalled by a red arrow, daily nutrients addition (culture medium) are signalled by black arrows.

Table 3.1 - Variations in frequency and dissipation of the experiment reported in fig. 3.1. $_B$= beginning of the experiment, $_E$= end of the experiment.

	Δf (Hz)			
Day 1	(f_{DAY1}- f_B)	-61.5 ± 1	(f_{DAY1}- f_B)	-61.5 ± 1
Day 2	(f_{DAY2}- f_B)	-109.7 ± 1.2	(f_{DAY2}- f_{DAY1})	-48.1 ± 1.4
Day 3	(f_{DAY3}- f_B)	-153.0 ± 0.5	(f_{DAY3}- f_{DAY2})	-43.3 ± 1.2
Day 4	(f_{DAY4}- f_B)	-151.8 ± 0.9	(f_{DAY4}- f_{DAY3})	1,2 ± 0.9
Day 5	(f_{DAY5}- f_B)	-163.4 ± 0.7	(f_{DAY5}- f_{DAY4})	-11.6 ± 1.0
Day 6	(f_{DAY6}- f_B)	-172.6 ± 1.6	(f_{DAY6}- f_{DAY7})	-9.2 ± 1.6
	Total Δf (f_E- f_B)			-172.6 ± 1.6
	ΔD (dimensionless)			
Day 1	(D_{DAY1}- D_B)	6.6E-05 ± 2E-07	(D_{DAY1}- D_B)	6.6E-05 ± 2E-07
Day 2	(D_{DAY2}- D_B)	6.3E-05 ± 4E-07	(D_{DAY2}- D_{DAY1})	-3.5E-06 ± 4E-07
Day 3	(D_{DAY3}- D_B)	5.5E-05 ± 2E-07	(D_{DAY3}- D_{DAY2})	-7.1E-06 ± 4E-07
Day 4	(D_{DAY4}- D_B)	5.1E-05 ± 4E-07	(D_{DAY4}- D_{DAY3})	-4.6E-06 ± 4E-07
Day 5	(D_{DAY5}- D_B)	4.9E-05 ± 2E-07	(D_{DAY5}- D_{DAY4})	-1.6E-06 ± 5E-07
Day 6	(D_{DAY6}- D_B)	5.0E-05 ± 3E-07	(D_{DAY6}- D_{DAY5})	6.1E-07 ± 2E-07
	ΔD_{TOT} (D_E- D_B)			5.0E-05 ± 3E-07

3.1.1.1 The influence of the bacterial culture

The experiments performed in these conditions showed that even if there were not relevant differences at the end of the growth phase, the increasing of the mass during the first overnight growth in static conditions was considerably influenced by the freshness of the bacterial solution inoculated.

In Fig. 3.2 the first overnight growth of two experiments are reported. In both experiments a bacterial suspension of OD_{600} 0.2 was introduced in the chamber of the QCM. In the case of the blue curve, the suspension introduced in the chamber is obtained from an overnight culture of *E. coli* and Δf_{blue} is approximately -60Hz, while in the case of the orange curve, the suspension is obtained from a fresh culture and Δf_{orange} is approximately twice of Δf_{blue}.

This result is due to the fact that the optical density value is obtained without distinction between live and dead cells. In an overnight culture there are more dead cells than in a fresh culture, even if the optical density is the same. The fresh culture has more vital cells that are able to attach to the quartz and start to divide, for this reason, the achievement of the biofilm growth-plateau is faster.

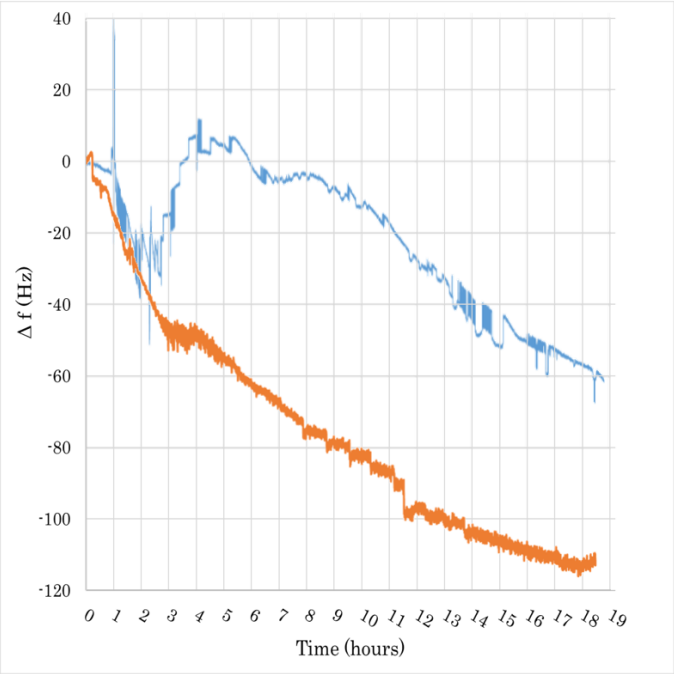

Figure 3.2 – Comparison between an overnight growth in the QCM in static condition after the introduction of a bacterial suspension OD_{600} 0.2 obtained from an overnight culture (blue curve) and a bacterial suspension OD_{600} 0.2 obtained from a fresh culture (orange curve).

3.1.2 Attach&Flow method

Another method to grow biofilms, the Attach& Flow method, was investigated. After a static phase to promote a first attachment of bacteria to the surface of the quartz, the sterile broth was pumped continuously throw the chamber, representing a constant supply of fresh nutrients and oxygen. With this method, there are no more stop and start of the flow that appeared to have consequences on the sample (see paragraph 1.1.1) removing a part of it daily.

In fig. 3.3 an example of monitoring of biofilm growth with the Attach&Flow method is reported, while in Table 3.2 the related variation in frequency and dissipation are illustrated.
It is possible to observe that the frequency signal doesn't decrease constantly, but it has fluctuations in the middle of each day. This phenomenon is due to the environmental temperature that reach the maximum at midday. Even if the instrument was placed inside an incubator, it was not possible to completely isolate the inner from the outer environment, as it was inevitable to let the connection cable and the tubes to exit.

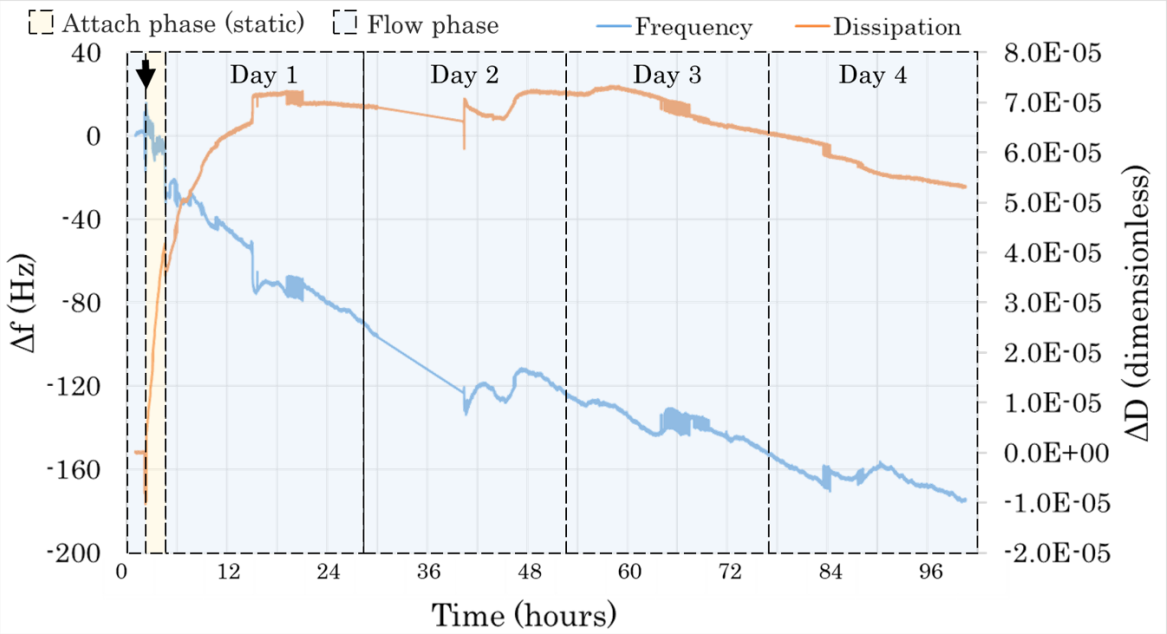

Figure 3.3 – Graph of an experiment performed with the Attach&Flow method. The first flow phase (light blue) corresponds to the signal of sterile MH broth collected in flow condition. The sample injection is highlighted with a black arrow. After the attach phase (yellow), it is possible to observe four days of growth in flow condition (light blue).

Table 3.2 – Variations in frequency and in dissipation of the experiment reported in fig. 3.3. $_{ASF}$= after the static phase, $_{B}$= beginning of the experiment, $_{E}$= end of the experiment.

	Δf (Hz)			
ASF	(f_{ASF}- f_B)	-31.2 ± 1.5	(f_{ASF}- f_B)	-31.4 ± 1.5
Day 1	(f_{DAY1}- f_B)	-92.7 ± 0.5	(f_{DAY1}- f_{ASF})	-61.7 ± 1.5
Day 2	(f_{DAY2}- f_B)	-126.0 ± 0.5	(f_{DAY2}- f_{DAY1})	-33.3 ± 0.6
Day 3	(f_{DAY3}- f_B)	-153.5 ± 0.4	(f_{DAY3}- f_{DAY2})	-27.5 ± 0.6
Day 4	(f_{DAY4}- f_B)	176.9 ± 0.5	(f_{DAY4}- f_{DAY3})	-23.4 ± 0.5
	Total Δf (f_E- f_B)			176.9 ± 0.5
	ΔD (dimensionless)			
ASF	(D_{ASF}- D_B)	3.7E-05 ± 4E-07	(D_{ASF}- D_B)	3.7E-05 ± 4E-07
Day 1	(D_{DAY1}- D_B)	6.9E-05 ± 1E-07	(D_{DAY1}- D_{ASF})	3.25E-05 ± 4E-07
Day 2	(D_{DAY2}- D_B)	7.2E-05 ± 1E-07	(D_{DAY2}- D_{DAY1})	2.7E-06 ± 2E-07
Day 3	(D_{DAY3}- D_B)	6.4E-05 ± 1E-07	(D_{DAY3}- D_{DAY2})	-8.0E-06 ± 2E-07
Day 4	(D_{DAY4}- D_B)	5.3E-05 ± 1E-07	(D_{DAY4}- D_{DAY3})	-1.1E-05 1E-07
	ΔD_{TOT} (D_E- D_B)			5.3E-05 ± 1E-07

The temperature fluctuations influence the signal and this effect is clearly visible in this experiment that is performed in a continuous flow condition. This is because the continuous flow avoids the removal of the biofilm caused by the switching of the flow, as in the Stop&Go method, that could mask the temperature effect.
Similarly to what has been observed in the experiments performed using the Stop&Go method, after the initial increase, the dissipation signal decreases day-by-day, signalling an overall hardening of the biofilm. For the first half of Day1, the dissipation had a trend that was specular to the one of frequency, then it decreased but recovered across the end of Day 2 and the first half of Day 3, when it reached its maximum. After its maximum, D decreased until the end of the experiment. The experimental conditions of Stop&Go and Attach&Flow methods are different, for this reason the two experiments are not precisely comparable. However, it is possible to make a consideration, by observing the data after 4 days of growth in both experiments: the overall behaviour recorded for frequency and dissipation along the two methods used in the experiments is similar, with comparable overall Δf (-176.9 ± 0.5 Hz for Attach&Flow, -151.8 ± 0.9 Hz for Stop&Go) and ΔD (5.3E-05 ± 1E-07 for Attach&Flow, 5.1E-05 ± 4E-07 for Stop&Go).

3.2 Real-time monitoring of biofilm growth and disinfection

The observation of the results of the preliminary experiments reported in paragraph 3.1 were used to design the experiments of the real-time monitoring of biofilm growth and disinfection. In particular, the Stop&Go method with a fresh inoculum was chosen to reduce the duration of the experiments.

Standard disinfectants for water applications and for medical sterilization have been chosen. In table 3.2, the disinfectant compounds and the related concentration tested are reported.

Table 3.2 – Disinfectant compounds and relative concentration used for the disinfection tests.

Disinfectant	Concentration
Amuchina (Sodium Hypochlorite)	0.45% in PBS (50ppm of Sodium Hypochlorite)
	0.9% in PBS (100ppm of Sodium Hypochlorite)
Aniosept Activ (Peracetic acid production in solution)	1% in MilliQ

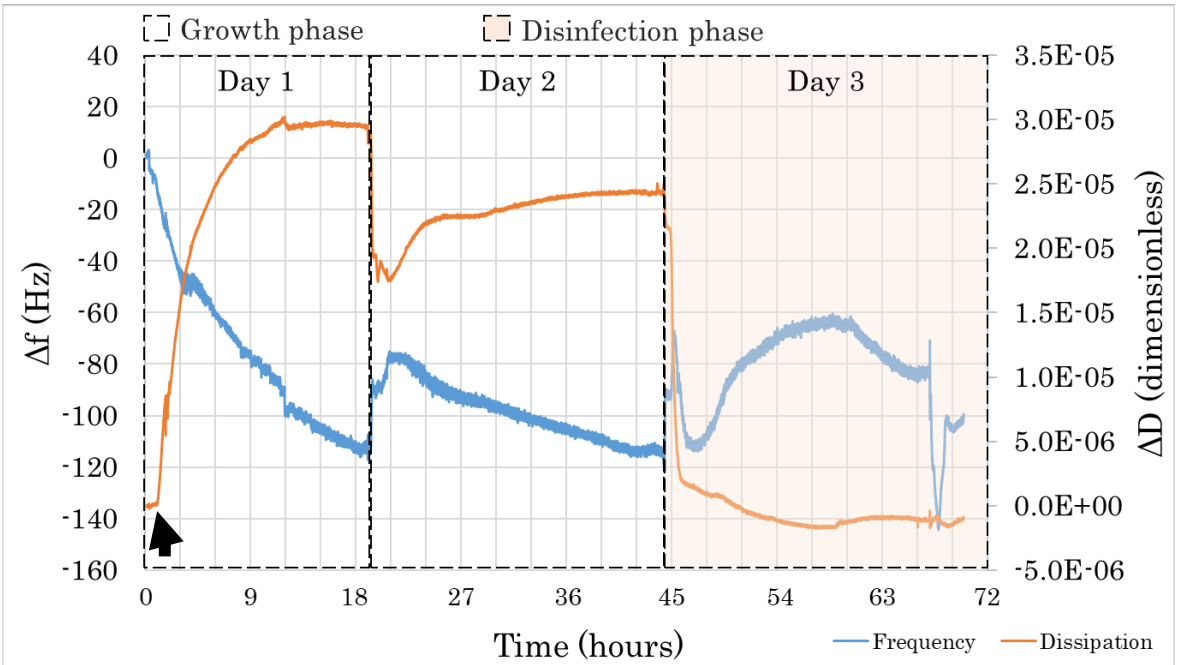

Figure 3.4 - Graph of an experiment performed with the Stop&Go method. The growth phase part of the graph is white, while the disinfection phase is in pink. The sample injection is highlighted with a black arrow.

Table 3.3 - Variations in frequency and dissipation of the growth phase of the experiment reported in fig. 3.4. B= beginning of the experiment, E= end of the experiment. Data about the disinfection phase are reported in the next page.

	Δf (Hz)		**ΔD (dimensionless)**	
Day 1	(f_{DAY1}- f_B)	-115.4 ± 0.6	(D_{DAY1}- D_{ASF})	2.9E-05 ± 7E-08
Day 2	(f_{DAY2}- f_{DAY1})	-1.2 ± 0.9	(D_{DAY2}- D_{DAY1})	-5.2E-06 ± 7E-08
	Total Δf (f_E- f_B)	-116.6 ± 0.7	ΔD_{TOT} (D_E- D_B)	2.4E-05 ± 7E-08

In Fig. 3.4, an example of experiment of real-time monitoring of biofilm growth and disinfection is reported. It is possible to observe both the growth (day 1 and 2) and the disinfection phase (day 3).

After the replacement of the medium of day 2, there was an increase in frequency probably due to the flow of the liquid and then the frequency started to decrease again, indicating an increase in mass on the quartz. Despite this, the total Δf remained almost unchanged.

In fig. 3.5 and 3.6, frequency and dissipation traces of the disinfection phase with the three different disinfectant compounds are grouped. As it can be seen, disinfection carried out with different chemicals lead to a change in frequency and in dissipation, depend on the substance and concentration applied.

Every disinfection phase was characterized by a maximum Δf during the static phase followed by a decrease in Δf. The time involved for the reaching of the maximum was differentiated by the type of disinfectant used.
The increasing in frequency at the beginning of the disinfection suggests that there is a loss in the deposit mass on the sensor. If this effect could be due to the mechanical action of the fluid during the flow phase, it has to be highlighted that the frequency reaches the maximum during the static condition. This means that the mass is further decreasing even in the absence of flow which let thinking that part of the biofilm is still detaching from the sensor surface.
The subsequent decrease in frequency after the peak means that the mass on the sensor starts increasing again, even if there is still the disinfectant in the chamber. This particular behaviour could be due to the fact that the disinfection was not effective, and the biofilm started to grow again. However, the dissipation signal has not the same trend as during the growth phase. In particular, the dissipation tends to keep constant till the end of the disinfection phase for all the experiments. Therefore, another hypothesis which can be considered in this case is that there are dead cells that are precipitating on the quartz.
As it is clearly visible in fig. 3.5, the trend of the frequency in the case of the two sodium hypochlorite solutions is the same, reaching the maximum Δf after about half an hour and then decreasing. It has to be noticed that $\Delta f_{0.45\%}$ is less than half of $\Delta f_{0.9\%,}$ suggesting that the action of the disinfectant is concentration-related.
On the other hand, the trend of Aniosept Activ appears different from the trends exhibited by the Amuchina solutions, leading to the maximum Δf after about 12 hours. This might be due to a different mechanism of action. Though the maximum Δf gained with Aniosept is similar to the one reached with Amuchina 0.45%, the Δf at the end of the disinfection is higher in the case of Aniosept, indicating a better efficiency.

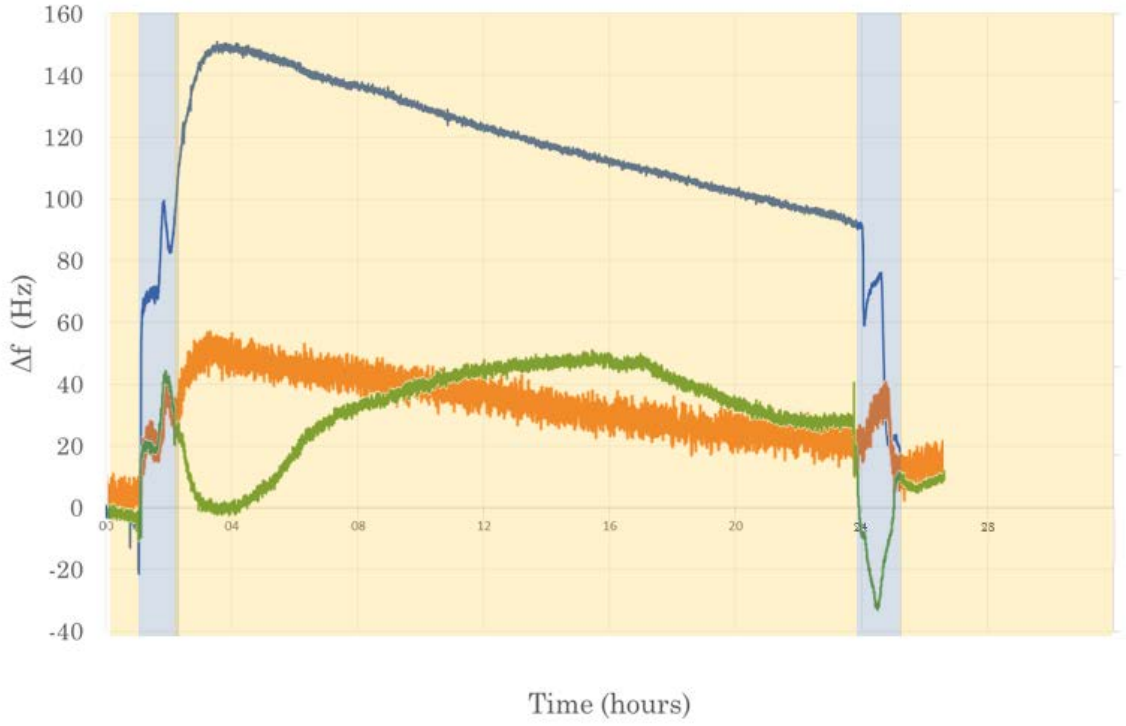

Figure 3.5 – Frequency signals of the three experiments reported together. Orange curve= Amuchina 0.45%, blue curve= Amuchina 0.9%, green curve= Aniosept Active 1%.

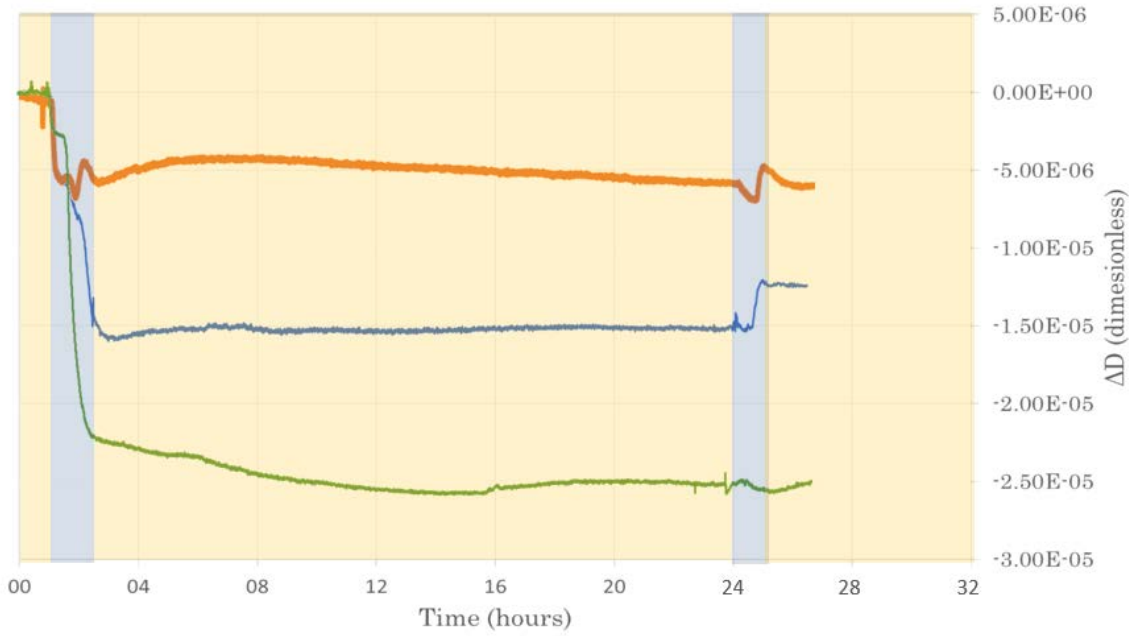

Figure 3.6 - Dissipation signals of the three experiments reported together. Orange curve= Amuchina 0.45%, blue curve= Amuchina 0.9%, green curve= Aniosept Active 1%.

After the reintroduction of sterile medium in the chamber, there is a decrease in frequency in all the cases. The dissipation value tends to remain constant in the case of Amuchina 0.45% and Aniosept Active, while it increases in the case of Amuchina 0.9% (fig. 3.6).

As the growth phase was performed in presence of MH broth, the medium was reintroduced in the chamber after the disinfection phase to provide a reference condition to compare disinfection and growth phase. It can be noticed that the frequency value after the re-introduction of broth was generally lower than the value immediately before.

The difference between the frequency after broth re-introduction and before the disinfection phase (Δf_{AB}) is not as significant as expected .(table 3.4). By considering Δf_{AB} as the frequency change due to the disinfection, it can be said that the activity of the three disinfectants doesn't show relevant differences as the frequency change due to the disinfection phase is between 12 and 14 Hz for all of them. This seems to suggest that every compound was not really effective and that there were not relevant differences between them. On the other hand, relevant disinfection effects have been observed during the static phase of the disinfection.

As a matter of fact, the trends in frequency and dissipation observed in the three cases along this phase indicated that there was a relevant interaction between the biofilm and the antibacterial compounds.

Table 3.4 - Variations in frequency and dissipation of the disinfection phases of the experiments reported in fig. 3.5. $_{AD}$= after disinfection, $_{BD}$= before disinfection, $_{AB}$= after broth introduction.

	Δf (Hz)		**ΔD (dimensionless)**	
Amuchina 0.45% (50 ppm of Sodium Hypochlorite)	(f_{AD}- f_{BD})	19.6 ± 2.1	(D_{AD}- D_{BD})	-5.6E-06 ± 1E-07
	(f_{AB}- f_{BD})	13.3 ± 2.4	(D_{AB}- D_{BD})	-5.4E-06 ± 1E-07
	(f_{AB}- f_{AD})	-6.2 ± 2.5	(D_{AB}- D_{AD})	1.8E-07 ± 7E-08
	Δf_{MAX}	48.8 ± 2.4	ΔD_{MIN}	-4.9E-06 ± 1E-07
Amuchina 0.9 % (100ppm of Sodium Hypochlorite)	(f_{AD}- f_{BD})	93.9 ± 0.9	(D_{AD}- D_{BD})	-1.5E-05 ± 5E-08
	(f_{AB}- f_{BD})	12.4 ± 0.9	(D_{AB}- D_{BD})	-1.2E-05 ± 4E-08
	(f_{AB}- f_{AD})	-81.5 ± 0.6	(D_{AB}- D_{AD})	2.7E-06 ± 4E-08
	Δf_{MAX}	151.0 ± 1	ΔD_{MIN}	-1.6E-05 ± 5E-08
Aniosept Activ	(f_{AD}- f_{BD})	30.7 ± 1.1	(D_{AD}- D_{BD})	-2.5E-05 ± 5E-08
	(f_{AB}- f_{BD})	12.3 ± 0.9	(D_{AB}- D_{BD})	-2.53E-05 ± 7E-08
	(f_{AB}- f_{AD})	-18.4 ± 1.1	(D_{AB}- D_{AD})	7.20E-08 ± 5.7E-08
	Δf_{MAX}	51.3 ± 1.5	ΔD_{MIN}	-2.6E-05 ± 6E-08

3.3 Points of criticism

The development and the optimization of the setup have proven to be challenging and took up a relevant quantity of time. The signals of quartz crystal microbalance are very sensible to the environmental conditions and requires a certain accuracy to gain repeatability, in order to compare results from different experiments or days. These aspects then need to match requirements of samples, in this case bacteria. For instance, an obstacle to the success of the experiments is the presence of air bubbles in the chamber. In fact, bubbles tend to get stack between the crystal surface and the chamber lid, creating an equivalent load on the sensor which influence the frequency and the damping of oscillations. In this case, the comparison between experiments would be impossible.

To reduce the risk of bubbles, it would be useful to degas the buffer, though the presence of oxygen in the medium is needed for the biofilm growth. For this reason, a refined setup design would be desirable.

As a temperature compensation curve for the sensor signal is not provided by the supplier, it is necessary to isolate the chamber and maintain a constant working temperature. In this study, the microbalance has been placed inside an incubator, however, it was impossible to guarantee a constant temperature due to the poor precision of the incubator temperature regulation system, and to the heat loss through the door caused by electrical cables and tubes linking the QCM to external parts of the setup. In addition, the tubes that were out of the incubator were at room temperature, so the incoming medium gave its contribution to the working temperature variations.

Last but not least, because of the design of the Open QCM^{-1}, the sterilisation of the chamber requires particular care, as the materials of the lid of the chamber are not autoclavable.

Solutions to improve the setup are illustrated in chapter 4.

Conclusions and perspectives

4

In this chapter the conclusions derived from the QCM study of bacterial biofilms are reported. Perspectives to further development of the study are proposed.

4.1 Conclusions

From experiments performed so far, the use of the QCM seems to be a valid strategy for the real-time investigation of biofilm formation and disinfection. The results obtained show that, in the case of both Stop&Go and Attach&Flow methods, the biofilm grow on the surface of the quartz reaches a maximum development probably due to the environmental and operational conditions given by the system.
Three different disinfectant compounds have been tested. The phenomenon observed during the disinfection phase is not fully understood and require further investigation, with particular regard to the differences observed before and after the broth re-introduction. However, it was possible to note that the disinfection phase proved to lead to modifications of the biofilm sample. During this phase in fact, the frequency increased at the beginning and then decreased, while the dissipation of the energy showed a decrease at the beginning and then kept constant. These trends correspond to:

- an initial loss in mass of the deposit, with a contemporary increase in stiffness,
- a subsequent increase in the mass deposit, likely due to dead cells precipitation on the sensor surface, further proved by a constant stiffness related to the attached remaining layer.

The quartz crystal microbalance has potential to be used for the monitoring of the disinfection processes, even if it is necessary to improve the setup that still have some limitations. Additional investigations are needed for a better understanding of some of the phenomena observed.

4.2 Perspectives

As mentioned in the previous paragraph, an improvement of the setup is necessary to optimize the experiments. Conducting the entire experiment inside an incubation room would solve the temperature issues.

Regarding the design of the experiments, the Attach&Flow method is a promising method that has been preliminarily explored. In fact, a continuous flow decreases the risk of perturbation of the system due to the intervention of the operator. It also represents a good method to deliver constantly the fresh nutrients required for the development of the biofilm.

As the biofilm is a heterogeneous structure that adapts easily to the environment, it is important to be able to maintain the working conditions to guarantee the repeatability of the study.

An evaluation of an alternative method to connect the tubes to the chamber is ongoing. Preliminary tests using disposable sterile needles have been performed. The insertion of these needles directly into the connectors of the top fluidic cover may represent the last step necessary to create a setup entirely made up by a sterile- disposable circuit.

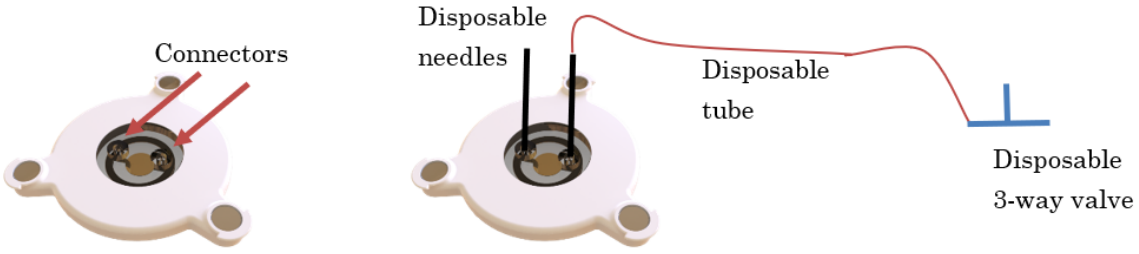

Fig. 4.1 – Schematic representation of a setup based on disposable circuit.

Lastly, by coupling the QCM chamber with a fluorescence microscope, a real-time visualisation of the biofilm could be performed in order to be able to observe what happens during the growth and the disinfection phases. The real-time visualisation of the biofilm could be then associated to vitality tests at the end of each experiment.

References

5

1. Gamry Instruments, I., Basics of A Quartz Crystal Microbalance. Rev. 1.2 1/27/2012.
2. analytik, T.; Available from: https://www.3t-analytik.de/technologies/qcm-d/what-qcm-d.
3. O'Sullivan, C.K. and G.G. Guilbault, Commercial quartz crystal microbalances – theory and applications. Biosensors and Bioelectronics, 1999. 14(8): p. 663-670.
4. Schofield, A.L., et al., Real-time monitoring of the development and stability of biofilms of Streptococcus mutans using the quartz crystal microbalance with dissipation monitoring. Biosensors and Bioelectronics, 2007. 23(3): p. 407-413.
5. Rodahl, M., et al., Simultaneous frequency and dissipation factor QCM measurements of biomolecular adsorption and cell adhesion. Faraday Discussions, 1997. 107(0): p. 229-246.
6. Sutherland, I.W., Biofilm exopolysaccharides: a strong and sticky framework. Microbiology, 2001. 147(1): p. 3-9.
7. Zhang, X., P.L. Bishop, and M.J. Kupferle, Measurement of polysaccharides and proteins in biofilm extracellular polymers. Water Science and Technology, 1998. 37(4-5): p. 345-348.

Part IV

Interaction between bacteria and silica nanoparticles

Introduction 1

Since bacterial biofilms are often undesirable, possibly harmful and they develop easily a resistance to disinfection treatments, the aim of this research was to investigate methods to detect them and to assess biofilm treatment effectiveness over the time. While a real-time approach has been discussed in Part III, an approach based on the morphology observation is illustrated in this part.

1.1 AFM for morphology studies

Using the AFM is possible to perform topographic analysis. Many imaging modes are available, among those the three main are the following:

- Contact mode, in which the tip is in contact with the sample and the probe-sample interaction is repulsive. This operation mode is applicable both in liquid and in air conditions and it has the advantage to allows fast scans with high resolution. On the other hand, its main disadvantage is the potential damage of both the probe and the sample.

- Non-contact mode. In this imaging mode, the tip is never in contact with the sample and the oscillation is due to tip-sample attractive forces. As the forces implicated are weak, there is no damage to the samples, for this reason this operation mode is suitable to softer samples. However, the separation between probe and sample involves a low lateral resolution. Measurements in air are favoured.

- Tapping mode is a hybrid method. There is the oscillation of the tip close to the fundamental frequency and it bounces down and up. In the lower position, the probe is in contact with the sample (repulsive forces) and then moves to the non-contact region. This method enables to obtain high lateral resolution and implies lower risks of sample damage.

Accordingly, the atomic force microscopy is a valid technique to perform morphology studies of various samples. Many experiments reported in literature applied AFM to bacterial cells, in order to investigate their structure and surface layers [2-7]. Providing good images of the bacterial structure and outer membrane, this technique can be used to compare bacterial cells before and after the exposure to particular environments or substances [8] .

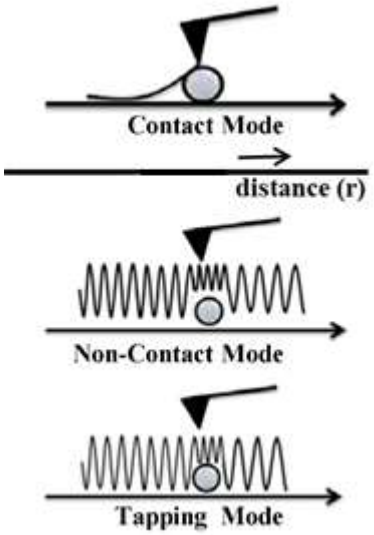

Figure 1.1- illustration of the three main imaging modes [1].

1.2 The advantages of using silica nanoparticles

Nanoparticles are investigated due to their antibacterial activity, metal oxides in particular [9-11]. There are many mechanisms of action of the nanoparticles, for instance, Sahoo et al. observed that gallium nitride nanoparticles were

damaging the outer membrane of bacteria and causing the spillage of intracellular components [12, 13]. Other mechanisms include reactive oxygen species formation, such as hydrogen peroxide [14], or interference with microorganism metabolism [15]. The characteristics of the nanoparticles, especially size and shape, are crucial for the bactericidal action [16].

Among the available nanoparticles, silica NPs are good candidates as antibacterial compounds. This is due to their biocompatibility, low toxicity for eukaryotic cells, their easy surface functionalization, and their availability with relatively low price [17, 18]. Furthermore, silica nanoparticles already demonstrated to have an antibacterial activity [19] and to induce a membrane damage in *E. coli* [7].

Materials and methods

2

In this chapter the materials and methods that have been used to study the interaction between bacteria and silica nanoparticles are reported.

2.1 Materials

In this study, the Gram-negative strain *P. fluorescens* ATCC 13525 was used. Mueller Hinton (MH) agar and broth for bacterial culture were purchased from Sigma Aldrich.
Commercial aqueous dispersed 100 nm silica nanoparticles (SiO_2-NPs-100nm) were purchased from Biovalley (France) and commercial aqueous dispersed 4 nm silica nanoparticles (SiO_2-NPs-4nm) from Alfa Aesar (France). The silica nanoparticles, with a Zeta potential around -50 mV, were used without functionalization.
Glass coupons were obtained from microscope slides (Fisherbrand Superforst) cutting 1 cm^2 squares using a diamond-tip pen. Ethanol absolute used for the dehydration of the samples was purchased from Sigma Aldrich. Millipore ultrapure water was used for nanoparticles suspension and for samples cleaning.

2.2 Bacteria and culturing

The stock of *P. fluorescens* was stored in glycerol (20%) at -80°C and used to inoculate Mueller Hinton agar plates. Colonies from the plates were inoculated in 20 ml of Mueller Hinton broth and let grow aerobically while shaken at 26°C overnight.

Glass coupons (1cm x 1cm) have been used as substrates to grow the biofilms in static conditions. The optical density at a wavelength of 600nm (OD_{600}) of the overnight culture of bacteria in MH broth was determined using a Helios gamma spectrophotometer (Thermo Scientific). The culture was then diluted to obtain an OD_{600}= 0.1 and used to cover the substrates. The samples were incubated at 26°C for 2 hours.

2.3 SiO_2 nanoparticles application

A combination of two sizes and different concentrations of SiO_2-NPs suspension were tested. The commercial suspension of SiO_2-NPs was diluted in MilliQ water to the chosen concentration and used to cover the samples that were therefore completely immersed for 2 hours.
In Table 2.1, the combinations of size and concentration of the SiO_2-NPs applied are reported.

Table 2.1 – Size and concentration of SiO_2-NPs

SiO_2-NPs	4 nm	1 g/L
		0.5 g/L
	100 nm	1 g/L
		0.5 g/L

2.4 Sample preparation for the morphology studies

The samples were fixed in glutaraldehyde (4% in PBS) for 1 hour, gently rinsed with MilliQ water and then dehydrated in increasing concentrations of ethanol solutions (25%, 50%, 75%, 90%, 100%), 10 minutes in every solution. After the dehydration, the samples were desiccated at 60°C for 10 minutes.

2.5 Morphology studies

Morphology studies were performed using a Bruker Nanoscope 2 with Nanoscope V controller. The instrument was mounted on an IX71 Olympus inverted optical microscope. The images were acquired in tapping mode in air (paragraph 1.1). Commercial rectangular silicon cantilevers with sharp tip

(Bruker NCHV-A) were used, with a nominal spring constant of 40 N/m and a nominal resonant frequency of 320 kHz. The images were collected at a scan rate of 0.2 Hz to 1.0 Hz, with a resolution of 512 x 512 pixels. Small forces were used, in order to prevent damages to the sample. For each acquisition, three channels were simultaneously generated: height, define as “the change in piezo voltage needed to keep the cantilever deflection constant”, amplitude error, namely “the difference between the cantilever oscillation amplitude and the amplitude setpoint” and phase, thus “the phase difference between phase of the cantilever oscillation read from the PSD and the phase of the drive signal sent to the tapping piezo. The phase signal includes the sample surface material properties information”[20].

2.6 Image processing

The images collected were then processed using Bruker Nanoscope Analysis software.

2.7 Acknowledgments

This study has been performed in collaboration with Biophyna team at LOMA laboratories (Laboratoire Ondes et Matière d'Aquitaine), Bordeaux, France.

Results and discussion

3

In this study, morphology studies were performed to assess if an interaction between *P. fluorescens* 2 hours old biofilms and silica nanoparticles occurs. In this chapter, the results are illustrated and discussed.

3.1 Bacterial morphology characterized by AFM

As reported in Part I- Chapter 1, the bacterial cell presents a cell wall composed of peptidoglycan. The cell wall makes the bacterial structure rigid, however during the dehydration there is a partial collapsing, and this helps to reveals the surface roughness [8, 21]. For the visualization of the real structure and size of bacteria, in liquid imaging is preferred because it maintains the cells hydrated. On the other hand, it reveals smoother surfaces, probably because the hydrated extracellular polysaccharides (EPS), that covers the bacterial cells, are soft and deformable [22]. Image acquisition in air permits to get a better resolution and visualize also the morphology of the outer membrane (OM) of bacteria.

In this study, the samples were fixed and then desiccated, and this procedure involves modifications. For this reason, observations were done by comparison between samples and controls that have been processed in the same way. Before performing the analysis of the interaction between bacteria and nanoparticles, preliminary tests on the visualization of structure and morphology of *P.fluorescens* using the AFM were performed. Two procedures of fixation and desiccation were compared with *in vivo* in liquid images.

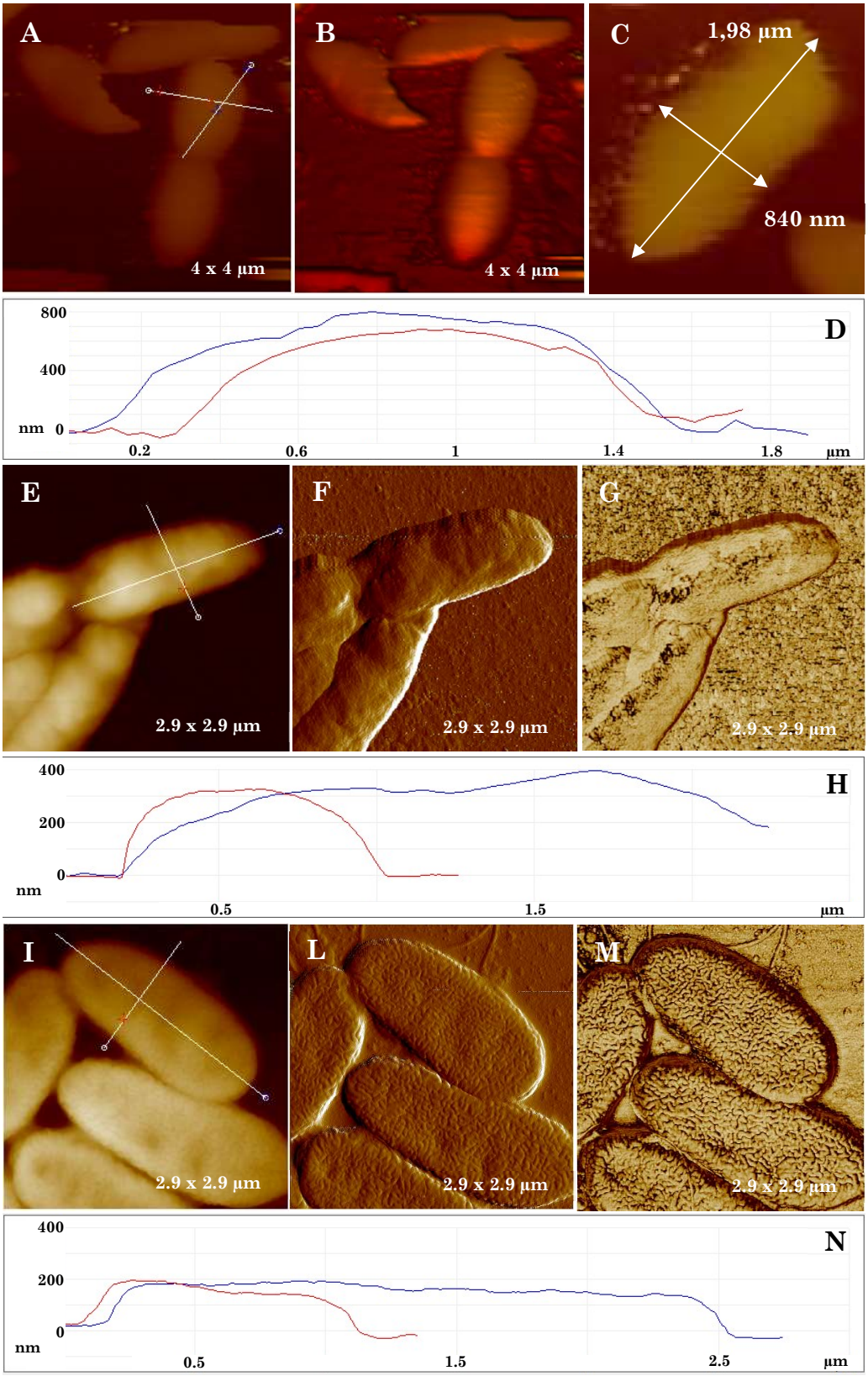

Figure 3.1 – AFM images of *P. fluorescens*: (A-B-C) height images in vivo in liquid with height cross-section (D); (E-F-G) height, amplitude and phase images of glutaraldehyde- fixed cells with height cross section (H); (I-L-M) height, amplitude and phase images of oven-desiccated cells with height cross section (N).

From the images collected *in vivo* in liquid, it was possible to observe that bacteria presented their typical rod-shape (fig. 1 A-B-C) with a size that resulted in the following average values: 1.80 µm length (ST. DEV. 0.22), 860 nm (st.dev. 111.15) width and 652 nm (st.dev. 22.68) height. In the case of both bacteria fixated in glutaraldehyde and desiccated in oven, there were not relevant variation in length and width, unlike in height. For bacteria fixated in glutaraldehyde (fig. 1 E-F-G), the average of height was 356 nm (st.dev. 53.57) (fig. 1H), almost half of the height measured *in vivo* in liquid (fig. 1D). The loss in height is even more visible in the samples desiccated in oven (fig. 1 I-L-M), that presented an average height of 194 nm (st.dev.27.21) (fig.1 N). It appears that the dehydration leads to a retraction in height that is less significant in the case of fixation with glutaraldehyde, indicating that the crosslinking action helps to preserve the structure during the dehydration phase. It also appears that in the case of biofilms desiccated in oven, without fixation with glutaraldehyde, the bacteria cannot maintain their original position on the substrate, and they passively migrate probably following the movement of the meniscus of the liquid during the desiccation, creating groups of cells attached one to the other one, as it is possible to observe in fig. 3.2.

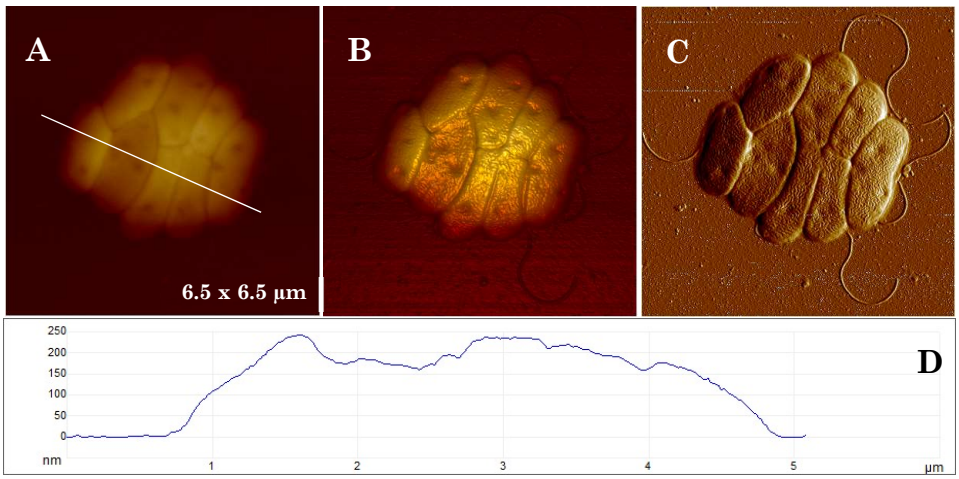

Figure 3.2 -Height (A), with cross section (D), height-3D (B)and amplitude (C) AFM images of *P. fluorescens* desiccated in oven for 1 hour. The cells appear stuck together, probably because of the movement of the liquid during the desiccation.

The surface of bacteria showed a "brain like" structure, which consists in ripples domains, according with what reported in literature for rod-shaped bacteria [7]. This pattern is due to the OM of the cell, as *P. fluorescens* is a Gram-negative bacterium (the structure of the Gram-negative cells is reported in Part I-Chapter 1).

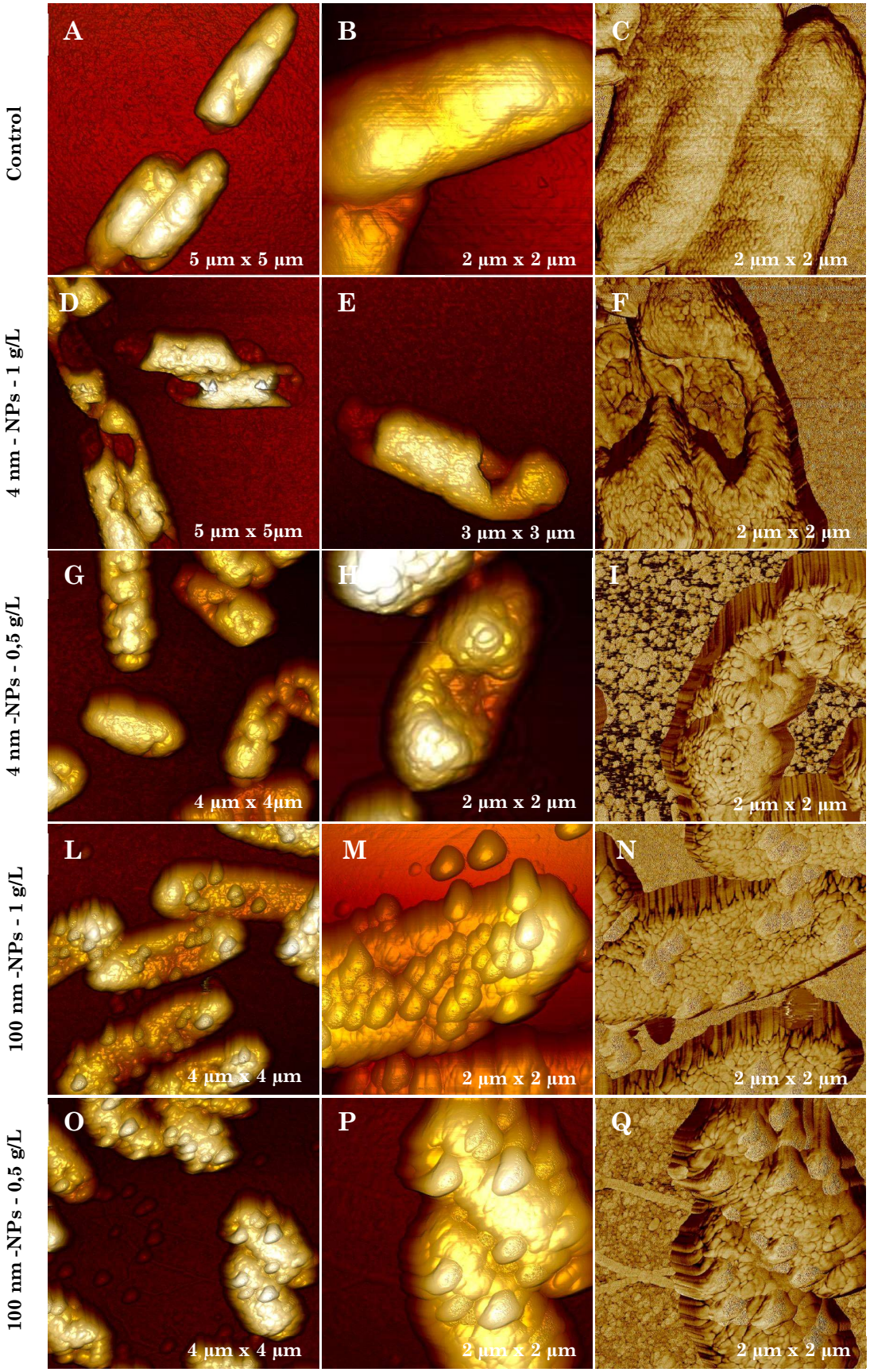

Figure 3.3 – AFM images of *P. fluorescens* treated with 4nm and 100 nm SiO_2NPs The samples have been fixated using glutaraldehyde. The study of the cross sections showed an average height of 356 nm (st.dev. 53.57).

3.2 Interaction between bacteria and silica NPs

In the case of 100 nm SiO_2-NPs, the images collected by AFM showed single NPs and aggregates both on bacterial cells and on the substrate. The nanoparticles look brighter than bacteria in the phase images and this effect is due to the higher rigidity. On the other hand, 4 nm SiO_2-NPs are not visible in AFM images because of their small size.

After the treatment with the 4 nm SiO_2-NPs the cells presented invaginations (fig. 3.3 D-E-F). These invaginations were mainly located in the extremities of the cells. After the treatment with 1g/L concentration, the bacteria appeared on average 60 nm longer than not-treated cells, but the extremities were spread on the substrate.

The height of the treated bacteria was on average 160 nm higher than not-treated cells. This is probably due to the fact that during the treatment there was an interaction that caused a swelling of the bacterial OM and wall first, and then a collapse. The average depth of the invaginations was 425 nm (st.dev 24.92) deep. In the case of 0.5 g/L (fig. 3.3 G-H-I), there were not relevant variations in length, but the same effect in the height was observable. The invaginations appeared less deep, with an average value of 106 nm (st.dev. 45.48).

For both the concentrations of nanoparticles suspensions, the "brain like" structure of the OM of the bacteria turned into an "island like" structure, showing that a reorganization of the membrane occurred (fig. 3.4).

In the case of 100 nm SiO_2-NPs, variation in the global morphology did not occur, but the same effect of reorganization of the outer membrane, as in the case of the 4 nm SiO_2-NPs was observable. The ripples nanodomains that were visible in the not-treated bacterial cells, were replaced by island-like structures in the exposed cells (fig.3 L-M-N-O-P-Q). Relevant differences on the effect were not observed between the two concentrations applied.

In a study reported in literature by Mathelié-Guinlet et al, in addition to membrane reorganization, evolution from a rod-shape to a spherical-shape of *E.coli* were observed after the treatment with 4nm SiO_2-NPs. On the other hand, after the exposure to 100nm SiO_2-NPs, modification at both levels were not observed [7].

These results are just partially comparable with those obtained in this research, exposing biofilms to SiO_2-NPs. The shape modifications observed after the exposure of *P. fluorescens* to 4nm SiO_2-NPs were completely different from those observed for *E. coli*, and the reorganization of the outer membrane was observed in the case of both 4nm and 100nm SiO_2-NPs.
These differences might be due to the fact that, even if *P. fluorescens* and *E. coli* are both Gram-negative bacteria, and therefore they show the same cell structure, there are biological differences that play an important role in the interaction with nanoparticles. In addition, while the study with *E. coli* was conducted with planktonic cells, this study was performed with bacteria adherent to a substrate (biofilm form). Particularly, the fact that bacteria were anchored to a surface may explain the reason why shape modifications were inhibited.

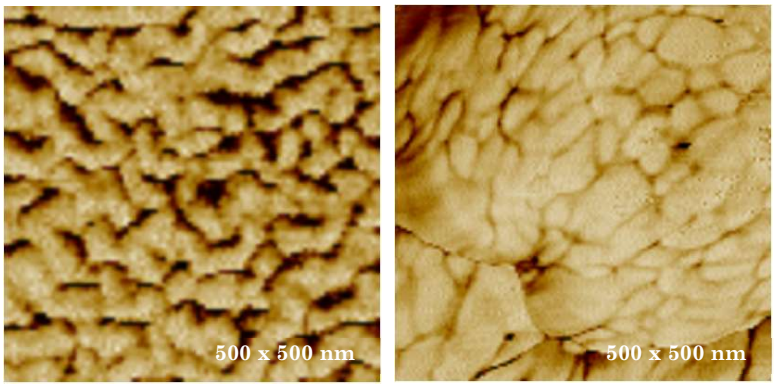

Figure 3.4 – Magnification of the OM of not treated *P. fluorescens* (left) that shows the "brain like" structure, and treated *P. fluorescens* (right) that shows the "island like" structure.

The invagination observed after the exposure to 0.5 g/L 4nm SiO_2-NPs (fig. 3.3 G-H-I) appear similar to the depression observed after antimicrobial peptides-treatments. This effect is due to the disruption of the bacterial outer membrane (OM) [23, 24]. The damages observed for the samples treated with 1 g/L 4nm SiO_2-NPs are more dramatic and led to a complete collapsing of part of the bacterial cell, suggesting that in this case the effect could be concentration-related.
The mechanism of the interaction observed is under study. Probably it is related to the composition of the outer cell membrane that is heterogeneous and includes lipids and proteins.

Results obtained by Jacobson et al., while investigating the interaction between gold nanoparticles and cell membranes (both *S. oneidensis*'s OM and artificial cell membranes), suggested that LPS (lipopolysaccharides) molecules are more adapt than other OM components to stick to nanoparticles that run up near the cell. It appears that the sticky attitude is directly related to the content of LPS, and also to the length of these molecules [25]. The study of interaction between nanoparticles and bacteria is a complex topic. Because of the wide variety of bacteria (each strain with its own characteristics), the comprehension of the mechanisms that lead to the action of the NPs is challenging. For instance, the relationship of "more NPs-bound means higher toxicity" is not necessarily valid because of the biological complexities [26]. Strain specific properties might involve different degree of action of NPs with antibacterial skills.

Vitality tests are required to be able to make accurate considerations about the bactericidal effect of the NPs that have been applied. However, considering the high damage occurred after the application of 4nm-NPs (invaginations and OM reorganization), while 100nm-NPs led just to the reorganization of the OM, it appears that the smaller nanoparticles have a higher toxicity. Size-depended effects have been observed for many types of nanoparticles, in particular for silver NPs.
For instance, Lu et al. observed that 5nm silver NPs have a higher bactericidal effect than 15 nm and 55 nm NPs [27], while Fujiwara et al. assessed that the toxicity of 5 nm silica NPs on *Chlorella kessleri* was higher than in the case of 26 nm and 78 nm [28].
The interaction mechanism is not completely understood, but it is due to the contact between the NPs and the bacterial surface; therefore, smaller NPs are more effective because they have a bigger surface available to get in contact with the cell membrane.

Conclusions and perspectives

4

In this chapter the conclusions derived from the study of the interaction between *P. fluorescens* 2h old biofilms and silica nanoparticles are reported. Perspectives to further development of the study are proposed.

4.1 Conclusions

Nanomaterials are investigated for biofilm treatment purposes. Among these, silica nanoparticles are promising, because of their characteristics of biocompatibility and low toxicity for eukaryotic cells. It has been observed their antibacterial activity throw the outer membrane damage.

From the results of this study, in fact, it is possible to assert that there is an interaction between silica nanoparticles and *P. fluorescens* grown on a glass substrate for 2 hours. Relevant damages have been observed in the morphology and in the organization of the membrane of the treated cells, compared to the not-treated cells. The mechanism is currently under study, but it appears to be related to the damage and reorganization of the outer membrane of bacteria, and in some cases the following collapse of part of the cell, which represents an evident signal of damage.
The protocol applied showed its usefulness to visualize if there was an interaction and an effect induced after a particular treatment, so it could be a benchmark for industrial treatments.

The most visible difference in terms of observable effects was between the two sizes of nanoparticles applied (4 nm and 100 nm), as the 4 nm SiO_2 NPs led to the partial collapse of cells, with a concentration-related effect. In the case of 100 nm SiO_2 NPs concentration- related differences were not observable. These results suggest the size-depended toxicity of the NPs.

4.2 Perspectives

From the results of this study it is possible to assert that there is an interaction between SiO_2 nanoparticles and the bacteria grown on a glass substrate for 2 hours. The NPs have a toxic effect causing relevant modifications of bacterial morphology, but vitality tests are necessary to confirm the bactericidal effect. It is necessary to determine what is the most effective size of SiO_2 NPs and the minimum concentration of NPs with a toxic effect. In this context, the understanding of the mechanism of action is important; on parallel, more investigations are necessary to predict the toxic effect that nanoparticles may have, allowing to design NPs with the highest possible efficiency and the minimum impact on the environment.

References

5

1. Marrese, M., V. Guarino, and L. Ambrosio, *Atomic Force Microscopy: A Powerful Tool to Address Scaffold Design in Tissue Engineering.* Journal of Functional Biomaterials, 2017. **8**(1): p. 7.
2. Schabert, F., et al., *Ambient-pressure scanning probe microscopy of 2D regular protein arrays.* Ultramicroscopy, 1992. **42-44**: p. 1118-1124.
3. Müller, D.J., et al., *Imaging purple membranes in aqueous solutions at sub-nanometer resolution by atomic force microscopy.* Biophysical journal, 1995. **68**(5): p. 1681-1686.
4. Ohnesorge, F., et al., *Scanning force microscopy studies of the S-layers from Bacillus coagulans E38-66, Bacillus sphaericus CCM2177 and of an antibody binding process.* Ultramicroscopy, 1992. **42-44 (Pt B)**: p. 1236-42.
5. Schabert, F.A. and A. Engel, *Reproducible acquisition of Escherichia coli porin surface topographs by atomic force microscopy.* Biophysical journal, 1994. **67**(6): p. 2394-2403.
6. Schabert, F.A., C. Henn, and A. Engel, *Native Escherichia coli OmpF porin surfaces probed by atomic force microscopy.* Science, 1995. **268**(5207): p. 92-4.
7. Mathelié-Guinlet, M., et al., *Probing the threshold of membrane damage and cytotoxicity effects induced by silica nanoparticles in Escherichia coli bacteria.* Advances in Colloid and Interface Science, 2017. **245**: p. 81-91.
8. Braga, P.C. and D. Ricci, *Atomic force microscopy: application to investigation of Escherichia coli morphology before and after exposure to*

cefodizime. Antimicrobial agents and chemotherapy, 1998. **42**(1): p. 18-22.

9. Kaweeteerawat, C., et al., *Toxicity of metal oxide nanoparticles in Escherichia coli correlates with conduction band and hydration energies*. Environ Sci Technol, 2015. **49**(2): p. 1105-12.
10. Lee, C., et al., *Bactericidal effect of zero-valent iron nanoparticles on Escherichia coli*. Environ Sci Technol, 2008. **42**(13): p. 4927-33.
11. Yoon, K.Y., et al., *Susceptibility constants of Escherichia coli and Bacillus subtilis to silver and copper nanoparticles*. Sci Total Environ, 2007. **373**(2-3): p. 572-5.
12. Sahoo, P., et al., *Probing the cellular damage in bacteria induced by GaN nanoparticles using confocal laser Raman spectroscopy*. Journal of Nanoparticle Research, 2013. **15**(8): p. 1-14.
13. Sharma, D., et al., *Synthesis of ZnO nanoparticles and study of their antibacterial and antifungal properties*. Thin Solid Films, 2010. **519**(3): p. 1224-1229.
14. Sirelkhatim, A., et al., *Review on Zinc Oxide Nanoparticles: Antibacterial Activity and Toxicity Mechanism*. Nanomicro Lett, 2015. **7**(3): p. 219-242.
15. Buszewski, B., et al., *The effect of biosilver nanoparticles on different bacterial strains' metabolism reflected in their VOCs profiles*. J Breath Res, 2018. **12**(2): p. 027105.
16. Raza, M.A., et al., *Size- and Shape-Dependent Antibacterial Studies of Silver Nanoparticles Synthesized by Wet Chemical Routes*. Nanomaterials (Basel, Switzerland), 2016. **6**(4): p. 74.
17. Asefa, T. and Z. Tao, *Biocompatibility of Mesoporous Silica Nanoparticles*. Chemical Research in Toxicology, 2012. **25**(11): p. 2265-2284.
18. Li, X., et al., *Biocompatibility and Toxicity of Nanoparticles and Nanotubes*. Journal of Nanomaterials, 2012. **2012**: p. 19.
19. Capeletti, L.B., et al., *Tailored Silica–Antibiotic Nanoparticles: Overcoming Bacterial Resistance with Low Cytotoxicity*. Langmuir, 2014. **30**(25): p. 7456-7464.
20. Bruker, *Expeiment guide: http://www.nanophys.kth.se/nanophys/facilities/nfl/afm/fast-scan/bruker-help/Content/Contact%20AFM/Advanced%20Contact%20Mode%20AFM%20Operation.htm*

http://www.nanophys.kth.se/nanophys/facilities/nfl/afm/fast-scan/bruker-help/Content/TappingMode%20AFM/TappingModeChannels.htm.

21. Gunning, P.A., et al., *Comparative imaging of Pseudomonas putida bacterial biofilms by scanning electron microscopy and both DC contact and AC non-contact atomic force microscopy*. Journal of Applied Bacteriology, 1996. **81**(3): p. 276-282.
22. Morris, V.J.A.K., A R%A Gunning, A P, *Atomic Force Microscopy for Biologists*. Atomic Force Microscopy for Biologists.
23. Li, A., et al., *Atomic force microscopy study of the antimicrobial action of Sushi peptides on Gram negative bacteria.* Biochim Biophys Acta, 2007. **1768**(3): p. 411-8.
24. Mularski, A., et al., *Atomic force microscopy of bacteria reveals the mechanobiology of pore forming peptide action.* Biochimica et Biophysica Acta (BBA) - Biomembranes, 2016. **1858**(6): p. 1091-1098.
25. Jacobson, K.H., et al., *Lipopolysaccharide Density and Structure Govern the Extent and Distance of Nanoparticle Interaction with Actual and Model Bacterial Outer Membranes.* Environmental Science & Technology, 2015. **49**(17): p. 10642-10650.
26. Buchman, J.T., et al., *Using an environmentally-relevant panel of Gram-negative bacteria to assess the toxicity of polyallylamine hydrochloride-wrapped gold nanoparticles.* Environmental Science: Nano, 2018. **5**(2): p. 279-288.
27. Lu, Zhong, et al., *Size-dependent antibacterial activities of silver nanoparticles against oral anaerobic pathogenic bacteria.* Journal of Materials Science: Materials in Medicine, 2013, p. 1465-1471
28. Fujiwara, Kitao et al., *Size-dependent toxicity of silica nano-particles to Chlorella kessleri*. Journal of Environmental Science and Health, Part A, 2008, p. 1167-1173

Final considerations

This PhD work aimed at looking for sensing methods enabling the monitoring of biofilm growth and of disinfection efficacy. To this end, the work was structured to carry out both cutting-edge and application-oriented research. A preliminary state-of-the-art analysis was conducted and led to focus on methods enabling to monitor nonspecific properties of biofilms, such as mass and mechanical properties.

According to these finding and requirements, an experimental activity on the use of the AFM to characterise the morphology and the mechanical properties of bacterial biofilms was carried out. In addition, the AFM experimental activity was complemented by a laboratory work on the performances of a QCM-based real-time system capable of monitoring the mass and the viscoelastic changes of biofilms along growth and disinfection.
Results of these activities indicate that there are opportunities in the following fields:

- novel disinfection treatments based on nanostructured materials;
- the understanding of interaction phenomena and effects associated to the exposure to disinfectants, by observing morphological changes at both cell and membrane levels;
- tuning of disinfectant application with the biofilm age to optimise the efficacy of the treatment;
- use of the QCM as reference sensor system for new resonant sensors, in order to characterise their response to biofilms.

Acknowledgements

The PhD project would not been possible without the support of family, friends and colleagues. I would like to thank in particular the team of the university of Trieste, prof. Cohen- Bouhacina and her team Biophyna of Loma Laboratories to make our collaboration possible and Prof. Canton from Ca'Foscari University of Venice for her precious help.
Thanks to my family and my friends for supporting and reassuring me during these three years.
And last, but certainly not least, I would like to thank my co-supervisors Prof. Sbaizero and Dott. Ing. Bertoni for supporting me during the entire PhD.